Geochimica et Cosmochimica Acta 388 (2025) 34–47

Contents lists available at ScienceDirect

Geochimica et Cosmochimica Acta

journal homepage: www.elsevier.com/locate/gca

Tracing the origin of volatiles on Earth using nitrogen isotope ratios in iron meteorites

Damanveer S. Grewal [a,b,c,*], Surjyendu Bhattacharjee [c], Gabriel-Darius Mardaru [c], Paul D. Asimow [c]

[a] School of Molecular Sciences, Arizona State University, Tempe, AZ 85281, USA
[b] School of Earth and Space Exploration, Arizona State University, Tempe, AZ 85281, USA
[c] Division of Geological and Planetary Sciences, California Institute of Technology, Pasadena, CA 91125, USA

ARTICLE INFO

Associate editor: Béatrice Luais

Keywords:
Nitrogen
Iron meteorites
Chondrites
Origin of volatiles
Earth

ABSTRACT

Understanding the relationships between the nitrogen (N) isotope ratios of early solar system planetesimals and terrestrial reservoirs is crucial for tracing the origin of volatiles on Earth. The Earth primarily grew from planetesimals and planetary embryos that accreted rapidly (within ~1–2 Ma after CAIs) in the inner solar system, also known as the non-carbonaceous (NC) reservoir. Magmatic iron meteorites, which sample the metallic cores of the earliest solar system planetesimals, have emerged as a promising proxy in this exercise. NC irons are distinctly ^{15}N-poor compared to their CC (carbonaceous or outer solar system) counterparts. However, the utility of this proxy is limited by the lack of knowledge of N isotope fractionation during core crystallization. Using high pressure-high temperature experiments, we show that equilibrium N isotopic fractionation between solid and liquid metal ($\Delta^{15}N^{solid-liquid} = \delta^{15}N^{solid} - \delta^{15}N^{liquid}$) is limited ($\leq$1.2 ‰) under conditions relevant for core crystallization. This, combined with the siderophile character of N and limited equilibrium N isotope fractionation during core-mantle differentiation, suggests that the δ^{15}N values of iron meteorites accurately represent the N isotopic composition of their parent bodies. Unlike the variation in the N isotope ratios of NC and CC chondrites, which can be attributed to the effects of parent-body processes acting on organic precursors, the ^{15}N-poor nature of NC irons relative to CC irons likely offers the most definitive evidence for the distinct N isotopic compositions of the earliest inner and outer solar system planetesimals. The N isotopic composition of Earth's primordial mantle ($\delta^{15}N = <-40$ ‰) suggests that it retains the memory of the early accretion of ^{15}N-poor NC iron meteorite parent body-like planetesimals. The early accreted ^{15}N-poor nitrogen may be stored in the deep mantle, segregated into the core, or lost to space during atmospheric loss caused by impacts. This signature was overprinted by the subsequent accretion and admixing of CC materials, which is reflected in the relatively ^{15}N-rich nature of Earth's atmosphere ($\delta^{15}N = 0$) and convecting mantle ($\delta^{15}N = -5$ ‰).

1. Introduction

The origin of nitrogen (N) on Earth is important for understanding the formation of habitable worlds within our solar system and beyond (Marty, 2012; Halliday, 2013; Hirschmann, 2016; Dasgupta and Grewal, 2019; Grewal et al., 2020; Suer et al., 2023; Tsuno et al., 2024). Comparisons between the N isotopic signatures of terrestrial and cosmochemical reservoirs serves as an important tool in this investigation. The N isotopic composition of Earth's mantle and atmosphere is distinct from that of proto-solar nebular gas and comets, but falls within the range observed in various classes of meteorites that sample early solar system planetesimals (Fig. 1) (Marty, 2012; Alexander et al., 2012; Halliday, 2013; Füri and Marty, 2015; Grewal et al., 2021c). This points towards a common origin of volatiles in early solar system planetesimals and in Earth. Due to their relatively primitive characteristics, chondrites are the preferred meteorites for elucidating this relationship. The N isotopic composition of volatile-rich CI and CM chondrites originating from the outer solar system (or the carbonaceous (CC) reservoir), is not very different from that of the accessible terrestrial reservoirs (Fig. 1) (Marty, 2012; Alexander et al., 2012; Halliday, 2013). Consequently, volatile-rich carbonaceous chondrites are generally believed to be the primary source of N in Earth. Even though CC materials are thought to

* Corresponding author at: School of Molecular Sciences, Arizona State University, Tempe, AZ 85281, USA.
E-mail address: damanveer.grewal@asu.edu (D.S. Grewal).

https://doi.org/10.1016/j.gca.2024.11.011
Received 2 August 2024; Accepted 9 November 2024
Available online 15 November 2024

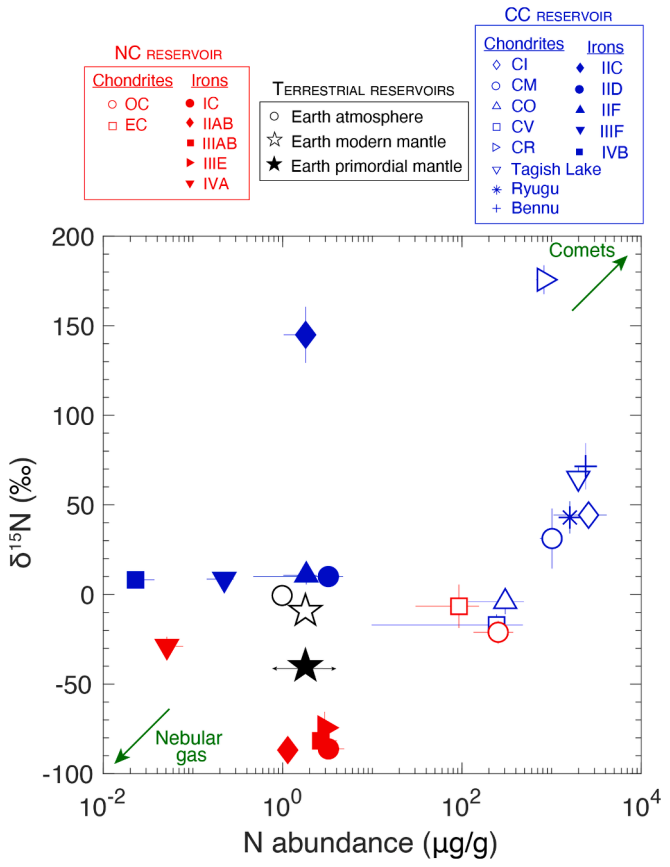

Fig. 1. $\delta^{15}N$ values of cosmochemical and terrestrial reservoirs plotted against their respective N inventories. The N isotopic composition of the terrestrial reservoirs lies within the range of meteorites and is distinct from the nebular gas and cometary reservoirs. Terrestrial reservoirs and iron meteorite parent bodies are N-depleted relative to chondrites. The $\delta^{15}N$ values of carbonaceous (CC; blue color) meteorites are generally higher than non-carbonaceous (NC; red color) meteorites. Note that the N inventory of Earth's primordial mantle is poorly constrained, as indicated by arrows. Data sources: Iron meteorite parent bodies (Grewal et al., 2021c, 2022b; Grewal and Asimow, 2023); Chondrites (Grady et al., 1986; Pearson et al., 2006; Alexander et al., 2012, 2013, 2018; Yabuta et al., 2023; Lauretta et al., 2024); Earth's primordial and modern mantle and atmosphere (Cartigny and Marty, 2013; Hirschmann, 2018).

contribute a small mass fraction towards the Earth's growth (Dauphas, 2017; Burkhardt et al., 2021), the N-depleted nature of terrestrial reservoirs compared to CC chondrites implies that even a small contribution from CC materials is sufficient to dominate Earth's N inventory.

The substantial presence of N in enstatite and ordinary chondrites (Grady et al., 1986; Hashizume and Sugiura, 1995), originating from the inner solar system (or the non-carbonaceous (NC) reservoir), however, suggests that Earth might not have obtained its N exclusively from CC materials (Fig. 1). The resemblance between the N isotopic composition of Earth's primordial mantle and ^{15}N-poor enstatite chondrites, and between Earth's atmosphere and ^{15}N-rich CC chondrites, has been used to argue for a mixed NC-CC reservoir origin for N on Earth (Javoy et al., 1986, 2010; Cartigny and Marty, 2013). This argument is based on a key assumption: that chondrite parent bodies originating from the NC and CC reservoirs have distinct N isotopic signatures, enabling the determination of the contributions of inner and outer solar system materials to the N budget of Earth. However, several lines of evidence suggest that this assumption may not be straightforward. All chondrites exhibit varying degrees of aqueous alteration and/or thermal metamorphism in their parent planetesimals (Brearley, 2006; Huss et al., 2006), and their N isotopic signatures appear to be affected by these processes (Alexander et al., 1998, 2007; Sephton et al., 2003; Foustoukos et al., 2021). Grewal (2022) showed that the $\delta^{15}N$ values and N content of bulk chondrites, as well as their insoluble organic matter (IOM) component, display a common correlation with their peak metamorphic temperatures, irrespective of their origin from NC or CC reservoirs. As the peak metamorphic temperature increases, both $\delta^{15}N$ values and N content decrease. This indicates that the N-bearing primordial materials in NC and CC chondrite parent bodies likely shared common origins, and the intra- and inter-group variations in the N isotopic compositions of chondrites reflect the effects of varying degrees of parent body processing (Sephton et al., 2003; Pearson et al., 2006; Alexander et al., 2017). In fact, the $\delta^{15}N$ values of the more thermally altered chondrites from the CC reservoir, i.e., CV and CO, fall within a similar range to enstatite and ordinary chondrites (Pearson et al., 2006; Alexander et al., 2018; Grewal, 2022). Thus, relying solely on chondrites to identify the locations of volatile reservoirs in the protosolar disk and tracing their contribution to the N budget of Earth is not ideal. Furthermore, meteorite evidence and planet formation models suggest that the building blocks of rocky planets began forming almost at the onset of solar system formation (Kruijer et al., 2014; Lichtenberg et al., 2021). For example, Mars likely formed within ~1–2 Ma after CAIs (Dauphas and Pourmand, 2011), and the building blocks of Earth could have formed within similar timescales (Rubie et al., 2011; Weidenschilling, 2011). Since chondrite parent bodies formed relatively late, >2 Ma after CAIs (Sugiura and Fujiya, 2014), they may not capture the N isotopic compositions of the earliest planetesimals in the NC and CC reservoirs, which were most likely the primary building blocks of terrestrial planets. To gain a more comprehensive understanding of this topic, further examination of a wider range of meteorites is necessary.

Recently, iron meteorites have emerged as a promising proxy to trace the N isotopic compositions of the earliest solar system planetesimals (Grewal et al., 2021c). Magmatic iron meteorites sample the metallic cores of the "first-generation" planetesimals (accreting within ~1 Ma after CAIs) from NC and CC reservoirs (Kruijer et al., 2017). The cores were formed as a result of planetesimal differentiation, involving extensive melting fueled by the decay of ^{26}Al (Hevey and Sanders, 2006; Sahijpal et al., 2007; Kaminski et al., 2020). Since N exhibits siderophile character at the oxygen fugacity (fO_2) relevant for iron meteorite parent body (IMPB) differentiation (IW − 3 to IW − 1; Grewal et al., 2024), it preferentially segregates into the metallic cores during core-mantle differentiation (Grewal et al., 2021c, 2022b). Consequently, the $\delta^{15}N$ values of iron meteorites are presumed to capture the bulk N isotopic signatures of differentiated planetesimals. The $\delta^{15}N$ values of iron meteorites have been analyzed over the last few decades by several research groups (Pepin and Becker, 1982; Franchi et al., 1993; Prombo and Clayton, 1993; Murty and Marti, 1994; Sugiura, 1998; Mathew et al., 2000; Ponganis and Marti, 2007). The mean $\delta^{15}N$ values of magmatic iron groups such as IC, IIAB, IIIAB, and IIIE from the NC reservoir lie within the range of –87 to –74 ‰, much lower than the mean $\delta^{15}N$ values of enstatite chondrites ($\delta^{15}N = -21.1 \pm 6.4$ ‰) (Fig. 1) (Grewal et al., 2021c). Given that terrestrial planets primarily grew by accreting early inner solar system planetesimals, which likely formed over similar timescales as NC IMPBs, the 50–70 ‰ difference between the $\delta^{15}N$ values of NC irons and enstatite chondrites can be an important constraint for tracing the origin of N in Earth. Meanwhile, the $\delta^{15}N$ values of CC irons are consistently higher than those of their NC counterparts, spanning the entire spectrum observed in CC chondrites (Fig. 1) (Grewal et al., 2021c; Grewal, 2022).

Since iron meteorites sample only the metallic cores, their utility in constraining the bulk N isotopic compositions of the earliest solar system planetesimals depends on the extent of N isotope fractionation during core-mantle differentiation and core crystallization. Limited N isotope fractionation during metal-silicate equilibration ($\Delta^{15}N^{metal–silicate} = \delta^{15}N^{metal} - \delta^{15}N^{silicate} = -3$ to -1 ‰) coupled with the siderophile character ($D_N^{metal/silicate} = [N]_{metal}/[N]_{silicate} = \sim 10–100$) of N at conditions relevant for planetesimal differentiation suggests that the N

isotopic signatures of bulk IMPBs closely resemble those of their parent cores (Grewal et al., 2022b). However, the effect of core crystallization on N isotope fractionation is unknown. The correlations between siderophile trace elements like Au, Ir, and As within iron groups are explained by fractional crystallization models primarily influenced by the S content in their parent cores (Wasson, 1999; Wasson and Richardson, 2001; Chabot, 2004; Wasson and Huber, 2006). These models suggest that S-rich liquids towards the end of the crystallization sequence are not sampled for most magmatic iron groups (Hilton et al., 2022; Zhang et al., 2022, 2024). Either magmatic iron meteorites sampling the later part of the crystallization sequence are missing in the meteorite record (Keil et al., 1994; Goldstein et al., 2009), or that crystallization halted prematurely, before reaching the Fe-Ni-S eutectic, due to early disruption of their parent bodies (Grewal and Asimow, 2023). Consequently, iron meteorites from most groups provide an incomplete representation of the bulk composition of their parent cores. Recent experimental studies show that there was substantial fractionation of N between solid metal and S-rich metallic liquids during core crystallization (Grewal and Asimow, 2023; Pathak and Dasgupta, 2024). This fractionation arises from the differences in the activity coefficient of N between the two phases, primarily due to the non-ideal interactions between N and S (Kunze et al., 1970). For instance, the activity coefficient of N in the Fe-Ni-C-N±S metallic liquids studied by (Grewal and Asimow, 2023) increases from 2.5 in S-free liquids to 5.8 in liquids containing ~25 wt% S. If these differences in activity coefficients are also reflected in the differences in the bonding environment of N between the two phases, resolvable N isotope fractionation between solid metal and S-rich metallic liquids should be expected during core crystallization.

In this study, we used high pressure-high temperature experiments to constrain the equilibrium N isotope fractionation between solid and liquid metal as a function of the S content in the metallic liquid. Utilizing our experimental data in combination with the $\delta^{15}N$ values of magmatic iron groups, we reconstruct the N isotopic composition of the parent cores and bulk IMPBs. Finally, we place the bulk N isotopic compositions of NC and CC IMPBs within the context of early solar system planetesimals from both inner and outer solar system reservoirs, providing insights into the origins of N on Earth.

2. Methods

2.1. Experimental details

2.1.1. Starting materials

The metallic mixtures consisted of varying proportions of Fe and S, with the N and Ni content held constant at 1.5 wt% and 10 wt%, respectively. The Ni content is in line with prior experimental research on trace element partitioning between solid and liquid metal (e.g., Chabot et al., 2017, 2006). Reagent-grade Fe, Ni, and $Fe_{3.32}N$ were combined with elemental S to produce starting mixtures labeled 3S (3 wt % S) and 8S (8 wt% S) (Supplementary Table 1). The reagent-grade powders were mixed in an agate mortar under ethanol for about 1 h, then left to dry overnight.

2.1.2. Experimental conditions

The experiments were performed at 1 GPa and 1175–1325 °C. Within this temperature range, Fe-Ni solid coexisted with Fe-Ni liquid containing 3–25 wt% S. We performed the experiments using an end-loaded piston cylinder device at Caltech with ½ inch CaF_2-crushable MgO assemblies. The experimental setup was identical to our previous study on this topic (Grewal and Asimow, 2023). Crushable MgO capsules were selected due to the inert nature of MgO toward metallic systems. Previous studies have shown consistent results for N isotopic fractionation between metallic and silicate melts, whether the capsules were enclosed inside Pt cylinders or not (Li et al., 2016; Shi et al., 2022; Grewal et al., 2022b). To maximize the amount of starting material for accurate measurements of $^{15}N/^{14}N$ ratios, the capsules were not enclosed in Pt cylinders. The starting materials were compressed into dense pellets using a 10-ton hand press to maximize material quantity. All experiments were sintered at ~850 °C for a few hours followed by heating to the target temperature. The sintering process is essential for reducing the porosity of the MgO capsules to minimize of N diffusion through the capsule walls (Grewal et al., 2021b, 2022b; Shi et al., 2022; Grewal and Asimow, 2023). The experiments were quenched isobarically.

2.2. Post- experiment sample preparation

In each experiment, the solid and quenched liquid phases fortuitously separated into two distinct cylinders with a clean division. This observation contrasted with our previous study using a similar setup (Grewal and Asimow, 2023), where the solid and quenched liquid, although completely separated, were still connected at the phase boundary. While the exact cause of this separation is unclear, it is likely related to the use of dense pellets as starting materials in this study. The clean separation of the two phases eliminated any risk of cross-contamination during sample preparation for N isotope analyses. Small slices of the solid and quenched liquid phases were cut longitudinally using a 30 μm diamond blade for electron probe micro-analysis. These slices were then mounted in Crystalbond™, ground with 1200 grit SiC, and polished with 0.3 μm alumina slurry. Finally, the polished samples were soaked in acetone overnight to remove the Crystalbond™. The uncut separated phases were crushed and finely ground in an agate mortar for bulk isotope analysis.

2.3. Analytical details

2.3.1. Electron Probe Micro-Analysis (EPMA)

The elemental compositions were obtained using a JXA-iHP200F field emission EPMA at Caltech (Supplementary Table 2 and 3), following the procedures outlined in Grewal and Asimow (2023). Uncoated conductive samples were placed on a double-side graphite tape attached to a glass disc. Pure Fe and Ni metal and natural troilite were used as standards for Fe, Ni, and S, respectively. A cohenite inclusion in iron meteorite and GaN, which served as secondary standards in Grewal and Asimow (2023), were used as standards for C and N, respectively. Since S-bearing liquids display heterogeneous textures on quenching, a beam size of 50–100 μm was used to determine their chemical compositions. We used an accelerating voltage of 12 kV and an emission current of 80 nA. Kα X-rays of C and N were measured with an LDE2 diffracting crystal (Grewal et al., 2019b, a, Grewal et al., 2021a). The counting time for N was 80 s on the peak and 60 s on each background, while other elements were measured with a counting time of 10 s on peak and 5 s on each background. We periodically reanalyzed Fe and FeS standards after every ~15 measurements to monitor potential C deposition effects. As reported in previous studies (Tsuno et al., 2018; Grewal et al., 2021b; Grewal and Asimow, 2023), the C blank in the standards remained stable over time at ~0.4–0.5 wt%. The C contents reported in the solid and quenched liquid metals were obtained after subtracting the corresponding C blanks in the Fe and FeS standards from the raw data of the experimental products.

2.3.2. Elemental Analyzer-Isotope Ratio Mass Spectrometry (EA-IRMS)

The N isotopic compositions of the solid and quenched liquid metals were measured using a Thermo-Fisher Flash Combustion Elemental Analyzer (EA) Isolink CN coupled to a Thermo Scientific Delta-V plus isotope-ratio mass spectrometer (IRMS) at Caltech over three analytical sessions. This technique has been used to previously to measure N isotope fractionation between metallic and silicate phases at a high precision of ±0.3 ‰ (1σ) (Grewal et al., 2022b). Moreover, this bulk analytical technique overcomes the issue with heterogeneity in the quenched liquid metal that would be associated with any microanalytical *in situ* approach. 3–4 μmole of N equivalents of metallic powders

were placed into a tin capsule. Samples were combusted in a quartz reactor packed with tungsten (VI) oxide, reduced copper and glass wool, set at 1020 °C with pulse of ultra-high purity O_2 at 200 mL/min. Gas from combustion reactor were sent to a reduction reactor packed with reduced copper and set at 650 °C and reduced to N_2. This N_2 was passed through a water trap (packed with magnesium perchlorate) to remove trace quantity water and subsequently through a gas chromatography column (packed with Porapak resin) to achieve chromatographic separation of N_2 from CO_2. He carrier gas was used throughout at flow rate of 100 mL/min. N_2 gases were then sent to IRMS for $^{15}N/^{14}N$ measurement. The measured N content in the combusted samples were almost identical to EPMA measurements, attesting for complete sample combustion. Nitrogen isotopic compositions of sample gases were calibrated to international standard air ($\delta^{15}N$ (‰) = $[(^{15}N/^{14}N)_{sample}/(^{15}N/^{14}N)_{atm} - 1] \times 1000$; $(^{15}N/^{14}N)_{atm} = 3.676 \times 10^{-3}$) using a reference gas ($\delta^{15}N_{atm} = 0.724$ ‰) measured before and after each sample gas. A series of in-house and international reference materials were used as standards to correct for further instrumental fractionations associated with combustion (see Supplementary Table 4 for isotopic compositions of reference materials). We attained a measurement precision of ± 0.08 ‰ (2σ) based on replicate standard analyses spanning each analytical session. Owing to a combination of factors such as higher N content of the analyte metal, thorough standardization, excellent chromatographic separation of N_2 peak, absence of instrumental drift, high degree of reproducibility of $\delta^{15}N$ of reference materials and excellence linearity of calibration curves (Fig. 2), the precision of our analyses was an order of magnitude higher than that of a previous study (Grewal et al., 2022b), where EA-IRMS technique was used to measure $\delta^{15}N$ of silicates and metals.

3. Results

3.1. Texture of experimental products

The S-bearing liquid metal, which was a uniform single phase at the target temperature, solidified into a dendritic texture upon quenching (Fig. 3A,B). The dendritic texture consisted of N-bearing Fe-Ni and FeS (Fig. 3C). The solid metal displayed a relatively uniform texture (Fig. 3D). No bubbles were observed in either the solid or quenched liquids of any experimental samples.

3.2. Equilibrium partitioning of N between solid and liquid metal

The equilibrium partition coefficient of N ($D_N^{solid/liquid}$), which accounts for its distribution between the solid and liquid phases, increases with higher S content of the liquid metal, as reported in previous studies (Grewal and Asimow, 2023; Pathak and Dasgupta, 2024) (Fig. 4; Table 1). This trend is also exhibited by C (Grewal and Asimow, 2023) and several other trace siderophile elements such as Ga, Ge, and Au (Chabot, 2004). Nitrogen tends to favor the liquid phase when the equilibrating liquid contained less than ~15–18 wt% S, but becomes compatible within the solid phase when the liquid contains more S (Fig. 4). The increase in $D_N^{solid/liquid}$ with S content is attributed to the rise in the activity coefficient of N with increasing S content in the metallic liquid (Grewal and Asimow, 2023). The $D_N^{solid/liquid}$ values observed in our study, conducted in a nominally C-free system, are comparable to those predicted by Grewal and Asimow (2023) for C-bearing systems (with up to 1 wt% C in the starting material) and are slightly higher than those of Pathak and Dasgupta (2024) for S-rich metallic liquids (>20 wt % S). Therefore, the non-ideal interactions between N and C do not appear to affect the $D_N^{solid/liquid}$ values within the range of C content in the metals studied by Grewal and Asimow (2023).

3.3. Equilibrium fractionation of N isotopes between solid and liquid metal

$\delta^{15}N^{solid}$ and $\delta^{15}N^{liquid}$ values range from −5.7 ‰ to −4.7 ‰ and −6.3 ‰ to −5.6 ‰, respectively, with a precision of ± 0.08 ‰ (2σ), based on replicate standard analyses across each analytical session (Table 1). Our experiments exhibit resolvable equilibrium N isotope fractionation between solid and liquid metal, with $\Delta^{15}N^{solid–liquid}$ (=$\delta^{15}N^{solid} - \delta^{15}N^{liquid}$) values varying between 0.3 ‰ and 1.0 ‰ (±0.12 ‰; 2σ based on the error propagation of the $\delta^{15}N$ values of the replicate standard analyses) (Fig. 5; Table 1). The solid metals had consistently higher $\delta^{15}N$ values than the equilibrating liquid metals, with the difference generally increasing with increase in the S content of the liquid metal. The positive correlation of $\Delta^{15}N^{solid–liquid}$ with S content of the liquid metal aligns with the trend of higher $D_N^{solid/liquid}$ values when the equilibrating liquid is S-rich (Fig. 4).

4. Discussion

4.1. Approach to equilibrium of N isotopes between solid and liquid metal

There are several indirect lines of evidence which suggest that N isotopes reached equilibrium between solid and liquid metals in our experiments. Nitrogen exhibits very high diffusivity in both solid (10^{-9} m^2s^{-1}; Oikawa (1982)) and liquid metal (10^{-8} m^2s^{-1}; Kojima et al., 1975) within the temperature range of our experiments. This high diffusivity is expected to result in the compositional and isotopic homogeneity of N over the mm scale of our experimental capsules within a few minutes. Previous experimental studies have demonstrated that, at the temperatures of our experiments, N achieves compositional equilibrium between solid and liquid metal within the experimental duration of this study (Grewal and Asimow, 2023; Pathak and Dasgupta, 2024). An experimental study on the equilibrium fractionation of Fe isotopes

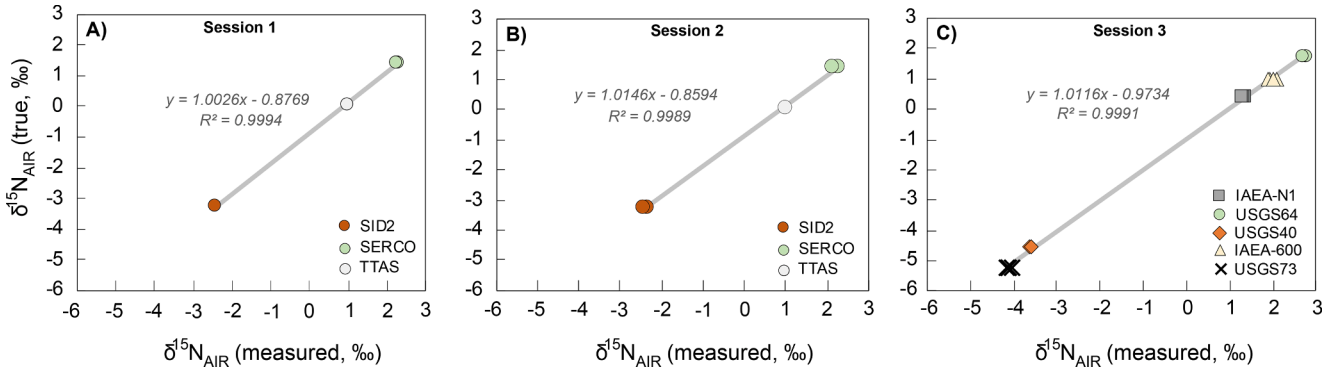

Fig. 2. Calibrations for N isotope measurement for each session (panels A: session 1; B: session 2; C: session 3) using in-house and international standards used to correct for instrumental fractionation effects.

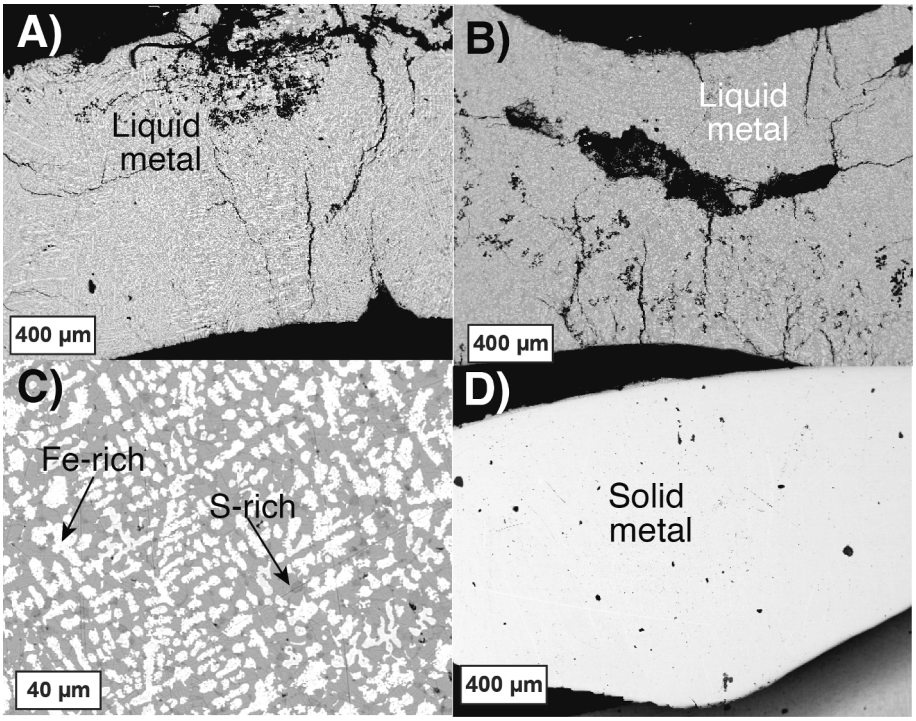

Fig. 3. Backscattered electron (BSE) images of experimental products. Panels A) and B) display the quenched textures of S-bearing metallic liquids. Panel C) displays the typical quenched texture of a S-bearing liquid at high magnification. Panel D) displays the texture of solid metal. Panels A), B), and D) also show the clean separation of solid metal from the liquid phase during quenching. A), C) = Exp. R634; B) = Exp. R639; D) = Exp. R620.

between solid and liquid metal has shown that isotopic equilibrium of Fe between these phases can be attained in under 24 h (Ni et al., 2020). Since the diffusivity of Fe in solid metal is ~3 orders of magnitude lower than that of N at the relevant temperatures (Mehrer, 2007), it is reasonable to expect that N isotopic equilibrium between solid and liquid metal should be achieved in much shorter timescales. The systematic trends of $D_N^{solid/liquid}$ and $\Delta^{15}N^{solid-liquid}$ with the S content of the liquid metal further indicate that compositional and isotopic equilibrium of N between the two phases were both achieved. In a recent experimental study on Cu isotope fractionation between solid and liquid metal, Ni et al. (2024) found that chemical equilibrium of Cu does not guarantee isotopic equilibrium between the two phases, especially in liquids with low S content (<20 wt% S). Considering the geochemical differences between Cu (a chalcophile element) and N (a siderophile element), as well as the distinct experimental conditions (low-pressure evacuated silica tubes vs. high-pressure piston cylinder), it remains uncertain whether similar challenges would affect the determination of N isotope equilibrium between solid and liquid metal. Further research, including time series experiments, is needed to address these concerns.

4.2. Effect of N deficit in experimental products on equilibrium fractionation of N isotopes between solid and liquid metal

In line with previous studies investigating the elemental and isotopic fractionation of N between metallic and silicate melts (Li et al., 2016, 2023; Dalou et al., 2017, 2019; Speelmanns et al., 2018, 2019; Grewal et al., 2019b, a, 2021b, 2022b; Jackson et al., 2021; Shi et al., 2022) and its elemental fractionation between solid and liquid metal (Grewal and Asimow, 2023; Pathak and Dasgupta, 2024), the N content in our experimental products is lower than of the starting materials. In experiments R629, R622, R620, and R634, the percentage of N retained ranges from ~77 % to 87 %, while experiment R639, which has the highest S content in the liquid metal, retained ~66 % of its initial N inventory. These retention rates are higher than or equal to those observed in Grewal et al. (2022b), where the effect of N loss on its equilibrium isotope fractionation between metallic and silicate melts was investigated. Through time series experiments, the authors demonstrated that N content and isotopic composition of metallic and silicate melts remained stable as a function of experimental duration, indicating no significant N diffusion through the capsule walls during equilibration. They proposed that the excess N was stored in the capsule pore spaces, suggesting that the system—comprising the capsule walls, metallic, and silicate melts—acted as a closed system. As a result, even with the N deficit in the experimental products, equilibrium fractionation of nitrogen isotopes was preserved. This conclusion was further supported by independent *ab initio* calculations. Based on the similarities in the experiment setup of Grewal et al. (2022b) and this study as well as the observed correlations between $\Delta^{15}N^{solid-liquid}$ and the S content in the liquid metal (Fig. 5), it can be inferred that our experimental products most likely reflect the equilibrium fractionation of N between solid and liquid metal. Further experiments with varying N levels in the starting materials and at different time durations are needed to validate our findings.

4.3. Cause behind N isotope fractionation between solid and S-bearing liquid metal

At the high temperatures relevant for core crystallization, the magnitude of equilibrium isotope fractionation of an element between two phases is controlled by the difference in its bonding environment in each phase (Young et al., 2015; Bourdon et al., 2018). In liquid iron, N and S atoms tend to repel each other because both occupy interstitial sites within the iron matrix (Hinomura and Nasu, 1998; Gaskell and Laughlin, 2017). This repulsion occurs because the presence of S atoms disrupts the local environment around N atoms, leading to increased repulsive forces. These repulsive forces are reflected in the increase in the activity coefficient of N with increasing S content in the liquid metal (Kunze et al., 1970). This explains the positive correlations observed between both $\Delta^{15}N^{solid-liquid}$ and $D_N^{solid/liquid}$ with increasing S content in the liquid metal (Figs. 4, 5). Since the difference in the bonding

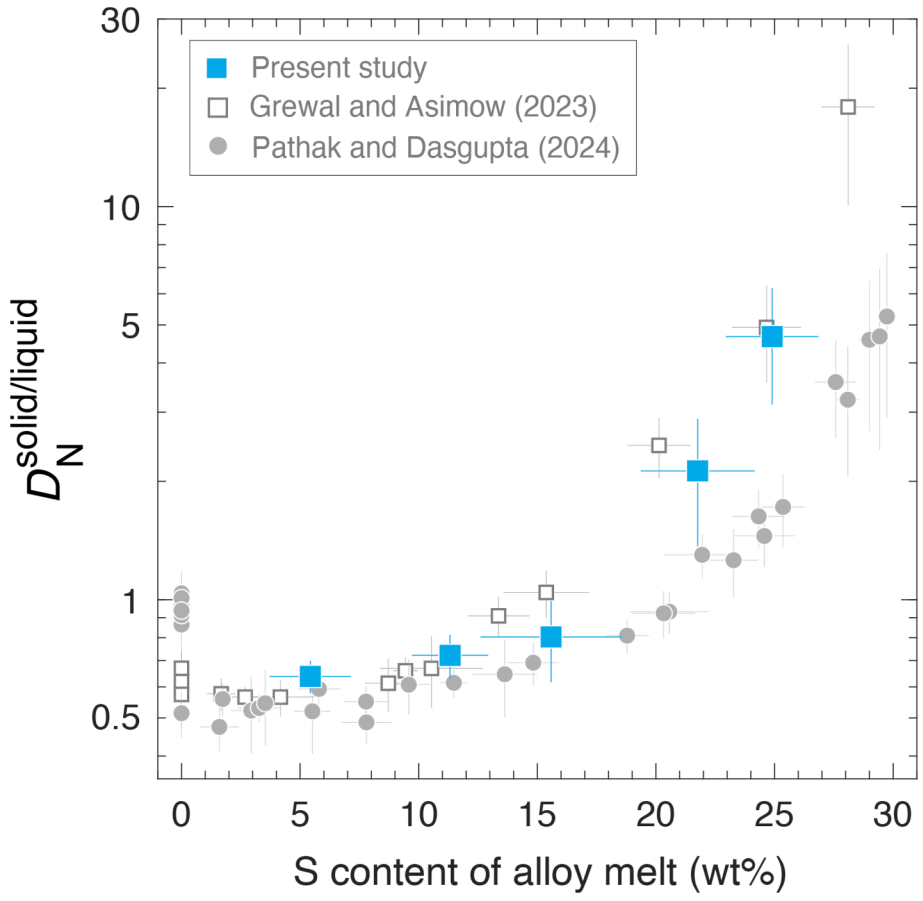

Fig. 4. $D_N^{solid/liquid}$ as a function of S content in the liquid metal. Nitrogen is incompatible in the solid metal when the S content of the equilibrating metallic liquid is below ~15–18 wt% S. Conversely, for higher S content, N becomes compatible in solid metal. Error bars for $D_N^{solid/liquid}$ and S content represent ± 1σ deviation, obtained by propagating the uncertainty from the standard deviation of replicate analyses of N and S contents in the samples.

Table1
Summary of experimental conditions, quench products, solid–liquid metal partition coefficients and isotope fractionation of nitrogen.

Exp	*P*	*T*	Time	Starting	Capsule	Quench Products	$D_N^{solid/liquid}$	1-σ	$\delta^{15}N^{solid}$	$\delta^{15}N^{liquid}$	$\Delta^{15}N^{solid-liquid}$
Samples	**(GPa)**	**(°C)**	**(h)**	**compositions**					**(‰)**	**(‰)**	**(‰)**
R629S	1	1325	6	Fe-10Ni-1.5N-3S	MgO	Solid metal+Liquid metal	0.35	0.06	−5.7	−6.0	0.3
R622S	1	1300	6	Fe-10Ni-1.5N-8S	MgO	Solid metal+Liquid metal	0.32	0.09	−5.4	−5.7	0.3
R620S	1	1250	6	Fe-10Ni-1.5N-8S	MgO	Solid metal+Liquid metal	0.80	0.19	−4.8	−5.6	0.8
R634S	1	1225	6	Fe-10Ni-1.5N-8S	MgO	Solid metal+Liquid metal	1.20	0.76	−4.7	−5.9	1.2
R639S	1	1175	6	Fe-10Ni-1.5N-8S	MgO	Solid metal+Liquid metal	0.66	1.54	−5.6	−6.3	0.7

environment of N between S-free solid and S-bearing liquid metal is less significant than between liquid metal and liquid silicate (metallic bonding of N in metals vs. covalent bonding of N in silicates), the magnitude of $\Delta^{15}N^{solid–liquid}$ (0.3 ‰ to 1.2 ‰) is lower than $\Delta^{15}N^{alloy–silicate}$ (−3 to −1 ‰; Grewal et al., 2022b)), even though the experiments in this study were conducted at lower temperatures.

4.4. Parameterization of N isotope fractionation between solid and liquid metal

Based on linear regression of the experimental data, the relationship between $\Delta^{15}N^{solid–liquid}$ and S content in the liquid metal can be described as:

$$\Delta^{15}N^{solid-liquid}(‰) = 0.03(\pm0.02) \times [S]_{liquid}(wt\%) + 0.3(\pm0.3) \quad (1)$$

Note that the experiments in this study were conducted at temperatures ranging from 1175 to 1325 °C. Ideally, to accurately isolate the effect of S, experiments should be conducted with varying S content in the starting materials while maintaining a constant temperature. However, as explained in Ni et al. (2020), this is not feasible because decoupling the effects of S content and temperature according to the Fe-Ni-S phase diagram requires substantial variations in the Ni content of the starting mixtures. Therefore, we adopted the alternate approach postulated by Ni et al. (2020), which involves correcting all equilibrium fractionation data to a single experimental temperature (e.g., 1250 °C for our study). Since equilibrium fractionation is inversely proportional to T^2 at high temperatures (Young et al., 2015; Bourdon et al., 2018), the $\Delta^{15}N^{solid–liquid}$ values are adjusted to a temperature of 1250 °C using the following equation:

$$\Delta^{15}N^{solid-liquid}_{1250°C} = \Delta^{15}N^{solid-liquid}_{T} \times \frac{[T(K)]^2}{[1250+273.15]^2} \quad (2)$$

The temperature-corrected $\Delta^{15}N^{solid–liquid}_{1250°C}$ values are slightly lower than the raw $\Delta^{15}N^{solid–liquid}$ values of low temperature ($T < 1250$ °C), S-

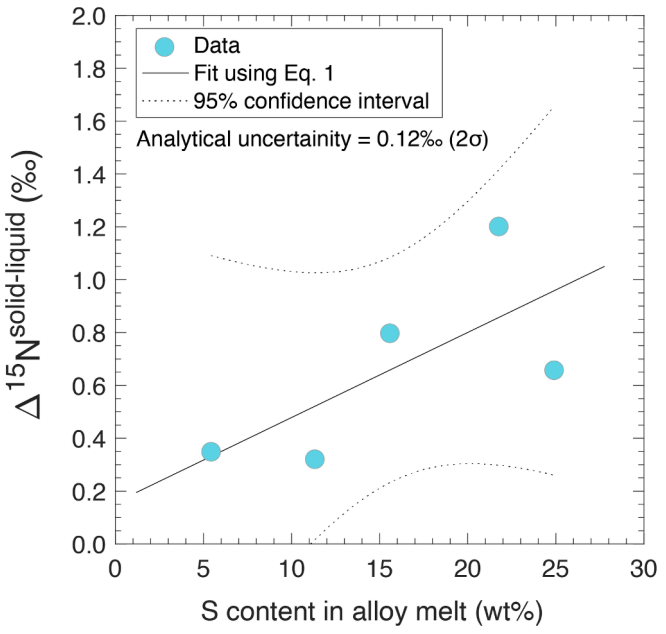

Fig. 5. $\Delta^{15}N^{solid-liquid}$ as a function of S content in the liquid metal. The solid metals are systematically ^{15}N-rich relative to the equilibrating S-bearing liquids and the magnitude of the fractionation appears to increase with higher S content in the equilibrating liquid. The solid line shows the best-fit correlation between $\Delta^{15}N^{solid-liquid}$ and S content in the liquid metal, based on Equation (1). The dashed line indicates the 95 % confidence interval for the regression.

rich liquids and higher than those of their high temperature ($T > 1250$ °C), S-poor counterparts. The difference between the raw and temperature-corrected values is fairly small, ranging from ~3–10 % relative. Using a simple empirical relationship derived from the linear regression of the temperature-corrected $\Delta^{15}N^{solid-liquid}_{1250°C}$ values at 1250 °C, the relationship between temperature-corrected $\Delta^{15}N^{solid-liquid}$ and S content in the liquid metal can be described as:

$$\Delta^{15}N^{solid-liquid}_{1250°C} = 0.03(\pm0.02) \times [S]_{liquid}(wt\%) + 0.2(\pm0.3) \quad (3)$$

4.5. Estimating the bulk N isotopic compositions of the parent cores and IMPBs

Here we use our experimental data to constrain the equilibrium fractionation of N isotopes between solid and liquid metal under conditions relevant for core crystallization in IMPBs. The increase in $\Delta^{15}N^{solid-liquid}$ with the S content of the equilibrating liquid suggests that S-rich liquid metal in equilibrium with solid metal can result in resolvable fractionation of N isotopes. Given that S-rich liquids, forming the latter stages of core crystallization for most iron groups, are absent in our meteorite record (Hilton et al., 2022; Zhang et al., 2022, 2024), we can use our experimental data to establish the bulk N isotopic composition of the parent cores. In this sub-section, we use the empirical $\Delta^{15}N^{solid-liquid}$ relationships (Eqs. (1) and (3) along with the mean $\delta^{15}N$ values of magmatic irons to estimate the $\delta^{15}N$ values of the parent cores and, consequently, the $\delta^{15}N$ values of bulk IMPBs.

Correlations among the abundances of siderophile elements (e.g., Ge, Ga, Au, As, and Ir) within magmatic iron groups can be explained by simple fractional crystallization models, where the equilibrating liquid becomes S-rich with increasing fractional crystallization (Chabot and Jones, 2003; Chabot, 2004). However, $\delta^{15}N$ values within grouped magmatic irons, similar to N and C abundances (Grewal and Asimow, 2023), do not show trends that are reminiscent of fractional crystallization (Fig. 6) (Franchi et al., 1993; Prombo and Clayton, 1993). Similar observations have been reported for Ge isotopes in iron meteorites (Luais, 2007). Elemental abundances or isotope ratios show fractional crystallization trends only if there was minimal sub-solidus diffusion across the solidified layers (Campbell and Humayun, 2005; Chabot and Zhang, 2022). Nitrogen diffuses in solid metals at rates ~3–4 orders of magnitude higher than those of trace elements that show systematic fractional crystallization trends (Oikawa, 1982; Mehrer, 2007). The slow cooling of magmatic irons (<1 to >1000 K/Ma) (Goldstein et al., 2009), as evidenced by Widmanstätten patterns (Buchwald, 1975), likely facilitated extensive sub-solidus diffusion of N across the solid metal. The relatively rapid sub-solidus diffusivity of N allows it to diffuse across solid metal over tens to hundreds of kms in a few million years, distances comparable to the sizes of parent cores of IMPBs (Grewal and Asimow, 2023). Thus, while there was resolvable elemental and isotopic fractionation of N between solid and liquid metal during core crystallization, as predicted by our experimental data, these trends were likely erased by the sub-solidus re-distribution of N. Consequently, similar to N abundances, we cannot use traditional fractional crystallization models to predict the N isotopic composition of the missing portions of the cores.

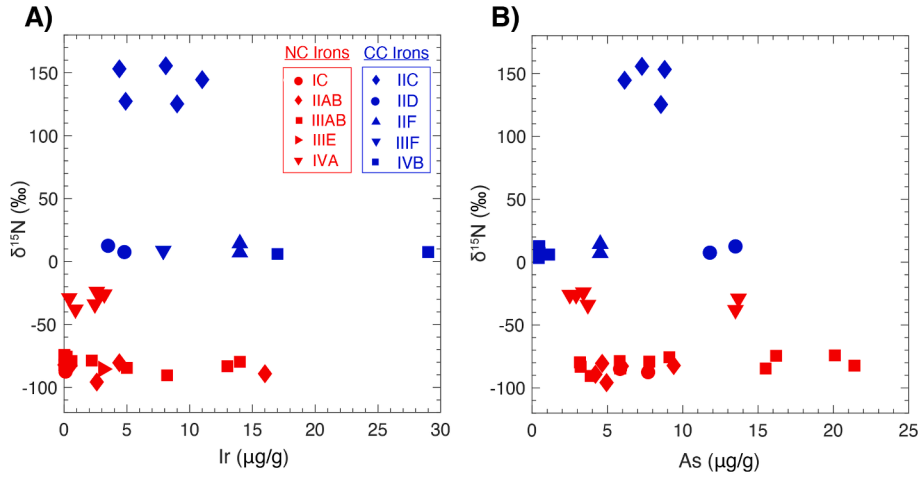

Fig. 6. $\delta^{15}N$ values of iron meteorites plotted against their A) Ir and B) As contents, which are indices of fractional crystallization. While many siderophile elements exhibit correlations with Ir and As, as expected in a fractional crystallization sequence, $\delta^{15}N$ values remain uncorrelated. Data sources: $\delta^{15}N$ – (Pepin and Becker, 1982; Franchi et al., 1993; Prombo and Clayton, 1993; Murty and Marti, 1994; Sugiura, 1998; Mathew et al., 2000); Ir and As – (Chabot and Zhang, 2022; Zhang et al., 2022, 2024).

Instead, we use a batch crystallization approach, similar to the one used for reconstructing the N and C abundances in the parent cores of IMPBs (Grewal and Asimow, 2023). Elemental and isotopic fractionation of N between solid and liquid metal, combined with the $\delta^{15}N$ values of magmatic iron meteorites, allows us to determine the N isotopic compositions of the parent cores by using the following set of equations:

$$\delta^{15}N^{core} = \frac{M_{solid} \times [N]_{solid}}{M_{solid} \times [N]_{solid} + M_{liquid} \times [N]_{liquid}} \times \delta^{15}N^{solid} + \frac{M_{liquid} \times [N]_{liquid}}{M_{solid} \times [N]_{solid} + M_{liquid} \times [N]_{liquid}} \times \delta^{15}N^{liquid} \quad (4)$$

$$\Delta^{15}N^{solid-liquid} = \delta^{15}N^{solid} - \delta^{15}N^{liquid} \quad (5)$$

$$D_N^{solid/liquid} = \frac{[N]_{solid}}{[N]_{liquid}} \quad (6)$$

$$f = \frac{M_{solid}}{M_{liquid}} \quad (7)$$

Mean $\delta^{15}N$ values of grouped irons reported in Grewal et al. (2021c) represent the N isotopic composition of the sampled core fractions ($\delta^{15}N^{solid}$). The ratio of the mass of sampled and unsampled core fractions (f) is determined based on the results of fractional crystallization models of siderophile trace elements (Hilton et al., 2022; Zhang et al., 2022). The S content of the parent core is combined with the mass fraction of the unsampled core to constrain its abundance in the missing conjugate liquid. This S content is used in parameterized $\Delta^{15}N^{solid-liquid}$ (either Eq. 1 or 3) and $D_N^{solid/liquid}$ (Grewal and Asimow, 2023) equations to determine the respective values of these parameters for each group. Combined, these equations estimate the bulk $\delta^{15}N$ values of each parent core ($\delta^{15}N^{core}$).

Our calculations show that the mean $\delta^{15}N$ values of the parent cores of grouped irons are within 0.1–0.5 ‰ of the mean $\delta^{15}N$ value of the iron meteorite samples from those groups (Fig. 7). For S-free cores (e.g., IVB), the mean $\delta^{15}N$ value of the parent core is within 0.1 ‰ of the mean $\delta^{15}N$ value of its meteorite samples due to the lower $\Delta^{15}N^{solid-liquid}$ value for S-free equilibrating liquid. The difference is larger for S-rich cores such as IC and IIAB, but not large enough to cause a substantial shift. To conclude, the mean $\delta^{15}N$ value of each parent core closely matches the mean $\delta^{15}N$ value of the iron meteorite samples from that group. Note that due to the low magnitude of N isotope fractionation between solid and liquid metal, the choice of which empirical relationship (Eq. 1 or 3) is used to determine $\Delta^{15}N^{solid-liquid}$ values does not significantly affect our results. Limited N isotope fractionation between metallic and silicate melts (Li et al., 2016; Grewal et al., 2022b) and the siderophile behavior of N at fO_2 relevant for planetesimal differentiation (Grewal et al., 2021b, 2022a) further imply that the $\delta^{15}N$ value of bulk IMPBs should closely resemble that of their parent cores, and consequently, iron meteorite samples from that group.

In summary, the N isotopic compositions of iron meteorites were not significantly altered either by solid metal-liquid metal fractionation during core crystallization (this work) or by liquid metal-liquid silicate fractionation during core-mantle differentiation (as shown by Grewal et al., 2022b). Importantly, the magnitude of these alterations are much lower than the intra-group variations of $\delta^{15}N$ values across magmatic iron groups. Therefore, N isotopic compositions of iron meteorites accurately reflect the bulk N isotopic compositions of their parent bodies

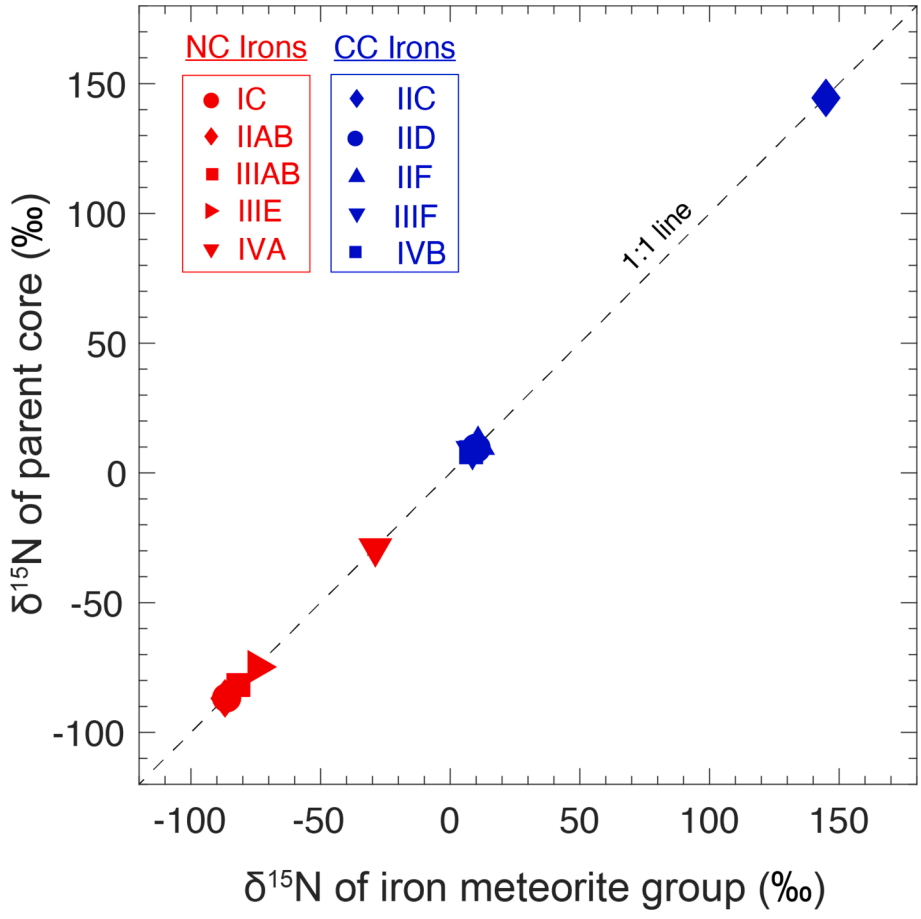

Fig. 7. The reconstructed $\delta^{15}N$ values of the parent cores of grouped magmatic irons plotted against the mean $\delta^{15}N$ values of iron meteorites. Due to the limited fractionation of N isotopes during core crystallization, the $\delta^{15}N$ values of the parent cores are nearly identical to those of the iron meteorites from the same group.

and can potentially serve as a reliable proxy for tracing the origin of N in terrestrial planets.

4.6. Variation in the N isotopic compositions of iron meteorites

Since magmatic iron meteorites sample the metallic cores of the earliest formed NC and CC planetesimals (Kruijer et al., 2014, 2017), their $\delta^{15}N$ values trace the N isotopic compositions of the "first-generation" planetesimals from both the inner and outer solar system reservoirs. Because the N isotopic compositions of iron meteorites are not affected by core crystallization and core-mantle differentiation, for simplicity, we will use the $\delta^{15}N$ values of magmatic iron groups reported in Grewal et al. (2021c) as representative of their parent bodies for further discussion in this study. The mean $\delta^{15}N$ values of 4 out of 5 magmatic NC iron groups (IC, IIAB, IIIAB, and IIIE) lie within the range of −87 to −74 ‰ (Fig. 1). These low $\delta^{15}N$ values are not observed in any group of chondrites originating from the inner solar system. For instance, the $\delta^{15}N$ value of the ^{15}N-poor enstatite chondrites is -21.1 ± 4.3 ‰. In contrast, IVA irons are comparatively ^{15}N-rich ($\delta^{15}N = -28.9 \pm 5.2$ ‰). The IVA parent core is depleted in N by more than an order of magnitude (0.3 μg/g) compared to other NC parent cores (5–14 μg/g) (Fig. 1) (Grewal and Asimow, 2023). It is also associated with anomalous depletion of moderately volatile elements, with Ga and Ge being depleted by one and three orders of magnitude, respectively, relative to other NC irons (Goldstein et al., 2009). Large variations in the metallographic cooling rates and Pd-Ag isotope systematics suggest IVA irons sample a core whose chemical composition was affected by large-scale volatile loss during catastrophic disruption of its parent body (Yang et al., 2007, 2008; Matthes et al., 2018). The higher $\delta^{15}N$ value of IVA irons could be a result of such disruption event.

The $\delta^{15}N$ values of the magmatic CC irons are consistently higher than those of their NC counterparts. Specifically, the mean $\delta^{15}N$ values of 4 out of 5 CC iron groups (IID, IIF, IIIF and IVB) lie within a narrow range of 8 to 11 ‰ (Fig. 1). These values are higher than the mean $\delta^{15}N$ values of CO, CV, and CK chondrites and lower than those of CI, CM, CR, and Tagish Lake (Grewal, 2022). Note that, like IVA irons, the anomalously N-, Ge- and Ga-depleted IVB irons (0.5 μg/g N content) were also affected by secondary volatile loss following disruption of their parent body (Yang et al., 2008). However, unlike IVA irons, its $\delta^{15}N$ value does not appear to be influenced by volatile depletion, implying that volatile loss in IVA and IVB cores may have occurred through different mechanisms. In contrast, the $\delta^{15}N$ value of the IIC irons is substantially higher (144.9 ± 15.6 ‰). The bulk N content of the IIC parent core (10 μg/g) is similar to the other CC parent cores such as IID and IIF (12–22 μg/g). The $\delta^{15}N$ value of the IIC irons is comparable to that of CR chondrites (175.7 ± 8.0 ‰), which are purported to capture the most primordial N isotopic composition amongst the CC chondrites (Fig. 1) (Alexander et al., 2013).

Overall, the $\delta^{15}N$ values of NC irons are consistently lower than CC irons (Fig. 1) (Grewal et al., 2021c). What caused the difference in the N isotopic compositions of NC and CC irons? Grewal et al. (2021c) proposed that this difference is due to the accretion of isotopically distinct N by NC and CC IMPBs. It was attributed either to the presence of isotopically distinct primordial carriers of N in the inner and outer parts of the protosolar disk, or the selective destruction of ^{15}N-rich carriers in the hotter, inner parts of the disk, resulting in NC IMPBs accreting ^{15}N-poor materials compared to CC IMPBs, despite the presence of common primordial materials of N in both reservoirs.

4.7. Comparisons between the N isotopic compositions of iron meteorites and chondrites

Unlike iron meteorites, the nitrogen isotopic compositions of chondrites from the NC and CC reservoirs do not show distinct differences (Grewal, 2022; Broadley et al., 2022). While CC chondrites tend to have higher $\delta^{15}N$ values than NC chondrites, there is significant overlap in the N isotopic compositions between certain groups of CC and NC chondrites. For instance, the mean $\delta^{15}N$ values of CR, Tagish Lake, Ryugu, Bennu, CI, and CM are systematically higher than NC chondrites, while the $\delta^{15}N$ values of CO and CV chondrites overlap with those of EC, OC, and RC chondrites from the NC reservoir (Fig. 1). This appears to contradict the notion of isotopically distinct N in inner and outer planetesimals, at least for those which accreted contemporaneously with chondrite parent bodies (Grewal, 2022; Broadley et al., 2022).

Nearly all of the N in chondrites is contained in organic matter, except in the anomalously reduced enstatite chondrites, where it is hosted in ultra-reduced, refractory phases such as osbornite (TiN), nierite (Si_3N_4), and sinoite (Si_2N_2O) (Grady et al., 1986; Alexander et al., 1998; Sephton et al., 2003). The heterogenous organic matter has broadly been classified into two categories – soluble organic matter (SOM) and insoluble organic matter (IOM) (Alexander et al., 2017). ^{15}N-rich SOM is susceptible to low-temperature (<300 °C) aqueous alteration and thermal metamorphism (Sephton et al., 2003). In contrast, IOM is relatively ^{15}N-poor and not easily altered by low-temperature parent body processes. A substantial drop in the bulk N content and $\delta^{15}N$ values has been observed in all classes of chondrites as a function of increasing alteration indices. For example, $\delta^{15}N$ values decrease with increasing degree of aqueous alteration in CM chondrites and with increasing thermal metamorphism in unequilibrated OCs, CO, and CV chondrites (Pearson et al., 2006; Alexander et al., 2013). This phenomenon is consistently observed in laboratory experiments when IOM and bulk CI-CM chondrites were subjected to hydrothermal alteration (Sephton et al., 2003; Alexander et al., 2007; Foustoukos et al., 2021). Grewal (2022) further demonstrated that the aforementioned decrease in bulk N contents and $\delta^{15}N$ values of NC and CC chondrites are well correlated with their peak metamorphic temperatures (Fig. 8A,B). This suggests that the parent bodies of chondrites, independent of their inner and outer solar system origin, likely accreted common organic precursors and their N isotopic compositions seem to be influenced by comparable geophysical processes.

The decay of ^{26}Al in early solar system planetesimals led to hydrothermal alteration, thermal metamorphism, and/or melting, with local temperature–time paths controlled by the competing effects of ^{26}Al decay-powered internal heating and conductive cooling at the surface (Hevey and Sanders, 2006; Sahijpal et al., 2007). Thermochemical models predict that relatively late accreting (>2 Myr after CAIs) planetesimals, akin to chondrite parent bodies, form onion-shell structures (Elkins-Tanton et al., 2011; Monnereau et al., 2013). Each layer within a planetesimal (i.e., depth in a 1D spherical model) follows a continuously varying temperature–time path, with lower peak metamorphic conditions in near-surface layers that are preserved as chondrites of low petrographic type and higher peak metamorphic conditions in deeper layers that are preserved as more equilibrated chondrites of high petrographic type (Sugiura et al., 1984, 1986; Monnereau et al., 2013). Similar geophysical processes powered by ^{26}Al decay in the early-forming NC and CC parent bodies can potentially explain the common correlation between N content and $\delta^{15}N$ values of NC and CC chondrites after the accretion of common organic precursors (Fig. 8). NC (enstatite and ordinary chondrites) and CC (CO and CV) chondrite parent bodies that formed within ~2–3 Myr after CAIs accreted substantial amounts of ^{26}Al and underwent significant parent body processing, which led to the preferential loss of ^{15}N-rich components. In contrast, other CC chondrite parent bodies (e.g., CI, CM, CR, Ryugu, Bennu, and Tagish Lake) formed later (>3.5 Myr after CAIs), accreted lower amounts of ^{26}Al, and underwent lower degrees of parent body processing, resulting in the preferential retention of ^{15}N-rich components. In this context, the lack of ^{15}N-rich NC chondrites in our meteorite record might reflect the absence of late-forming chondrite parent bodies in the inner solar system. Alternatively, it may be a sampling bias due to the dynamics of planetary growth in the inner solar system.

The interiors of IMPBs would also have followed similar temperature–time paths before large-scale melting and the gravitational

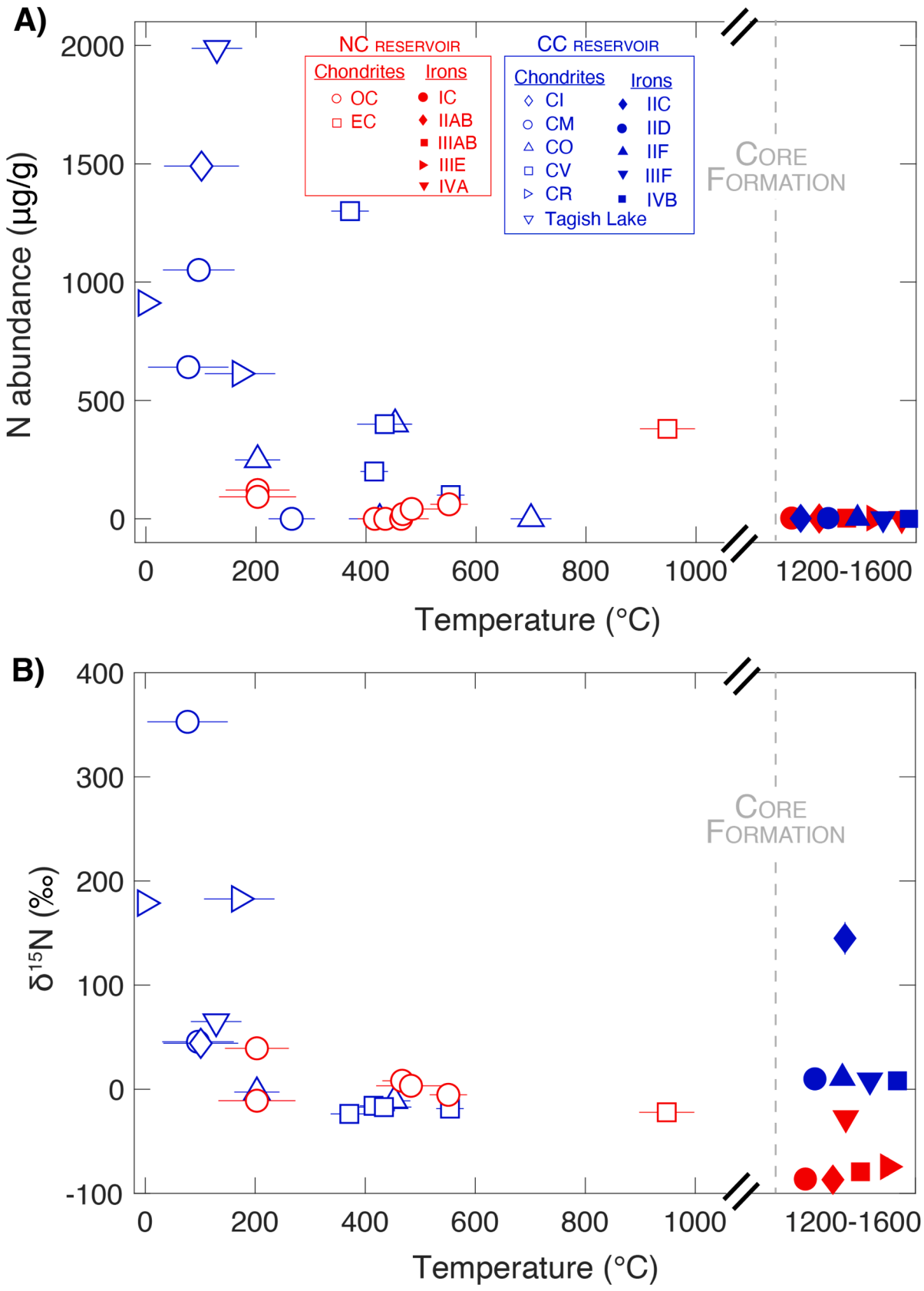

Fig. 8. N abundances and $\delta^{15}N$ values of bulk chondrites plotted against the peak metamorphic temperatures of chondritic samples inferred from organic thermometry (Cody et al., 2008). N abundances and $\delta^{15}N$ values of IMPBs, which experienced core formation at high temperatures (1200–1600 °C), are also plotted for comparison. N abundances and $\delta^{15}N$ values sharply decrease with increasing degree of thermal metamorphism and aqueous alteration at low temperatures (0–200 °C) and plot within a narrow range at higher temperatures. N abundances in IMPBs follow the same trend as chondrites. However, $\delta^{15}N$ values of IMPBs, unlike the narrow range shown by metamorphosed chondrites, exhibit large variations.

segregation of metallic droplets to form cores (Kaminski et al., 2020; Sturtz et al., 2022a,b). Efficient segregation of N into the core-forming metal during metal-silicate equilibration suggests that the $\delta^{15}N$ values of planetesimal cores must reflect the N isotopic compositions of the planetesimals at the final stage of their differentiation, i.e., temperatures higher than 1200°C (Grewal et al., 2022b). This is reflected in the N content of NC and CC IMPBs, which follow the overall trend of N depletion in bulk chondrites as a function of their peak metamorphic temperatures (Fig. 8A) (Grewal et al., 2022a). If NC and CC IMPBs, similar to chondrite parent bodies, accreted common organic precursors, then the N isotopic composition of their cores would follow the correlation between $\delta^{15}N$ values and peak metamorphic temperatures in chondrites. In other words, the $\delta^{15}N$ values of all cores (NC or CC reservoir parent bodies), should be in the range of −30 to −20 ‰, which is not observed (Fig. 8B). The $\delta^{15}N$ values of the parent cores of NC IMPBs are up to 50–70 ‰ lower than those exhibited by thermally metamorphosed chondrites, while the $\delta^{15}N$ values of IID, IIF, IIIF, and IVB irons from the CC reservoir are higher by 30–40 ‰. Notably, the $\delta^{15}N$ values of IIC irons lie in the range of 123–164 ‰, which is distinctly higher than that of the correlation based on thermal processing in chondrites. The $\delta^{15}N$ values of ungrouped CC irons such as Illinois Gulch (33.6 ‰), Mbosi (4.8 ‰), N'Goureyama (19.3 ‰), Nordheim (49.1 ‰), Sombrerete (37.3 ‰) and Tucson (8.2 ‰) (Prombo and Clayton, 1993), whose magmatic or non-magmatic origins are still uncertain, are also higher than those of the thermally metamorphosed chondrites. While new measurements of the $\delta^{15}N$ values of ungrouped irons could potentially fill in the gaps observed in the N isotopic compositions of grouped NC and CC irons, the wide variation in their $\delta^{15}N$ values (up to ~300 ‰) sharply contrasts with the narrow range of $\delta^{15}N$ values in metamorphosed (peak T > 300 °C) NC and CC chondrites.

What could explain this conflicting set of observations? Since the $\delta^{15}N$ values of the parent cores of IMPBs do not align with the correlation exhibited in chondrites, it is likely that IMPBs and chondrite parent bodies did not accrete similar N-bearing organic precursors. Additionally, the N isotopic compositions of NC and CC irons are distinct, with CC irons having systematically higher $\delta^{15}N$ values than NC irons. Primitive chondrites from the CC reservoir (e.g., CI, CM, CR, and Tagish Lake) also exhibit similarly high $\delta^{15}N$ values. However, the ^{15}N-rich components in these chondrites, in contrast to CC irons, are preferentially sequestered in labile phases which are highly sensitive to hydrothermal alteration. In traditional planetesimal core formation models, the elemental and isotopic composition of the core reflects the final equilibration event of metal with silicates at high temperatures (>1200–1400 °C) in magma ocean-like conditions (Hirschmann et al., 2021; Grewal et al., 2022a, b). The low $\delta^{15}N$ values of both bulk chondrites and IOM component of thermally metamorphosed chondrites attests to the fact that ^{15}N-rich components were easily lost during low temperature alteration (Grewal, 2022). If this is the case, how can the $\delta^{15}N$ value of the IIC irons be similar to that of isotopically primitive CR chondrites, and those of other CC irons such as IID, IIF, IIIF, and IVB within the range of primitive CM chondrites? A recent study has shown that both NC and CC IMPBs, based on their approximately similar oxidation states, must have experienced extensive hydrothermal alteration (Grewal et al., 2024b). This suggests that the accretion of common organic precursors by NC and CC IMPBs should result in the $\delta^{15}N$ values of their cores lying in a similar range, which is not the case. Therefore, the distinct N isotopic compositions of NC and CC IMPBs point towards the presence of isotopically distinct N-bearing precursors in the inner and outer parts of the protosolar disk. Since NC and CC IMPBs began to accrete right at the onset of solar system formation, the organic precursors, at least their N-bearing components, could have been different than what were accreted by the rather late-forming chondrite parent bodies. Further research is needed to better understand the origin and fate of organic carriers during the early stages of protosolar disk evolution, in context of spatio-temporal N isotopic variability of planetesimals.

In summary, the uniformity in the N isotopic compositions of thermally metamorphosed NC and CC chondrites, contrasting with the variation in the N isotopic compositions of the NC and CC irons, is an important observation (Fig. 8B). The correlation between the $\delta^{15}N$ values of NC and CC chondrites suggests that their parent bodies accreted common organic precursors and that variations in their N isotopic compositions reflect differential effects of parent body processing. Therefore, the N isotopic compositions of chondrites cannot be independently used to identify volatile reservoirs in the protosolar disk. In contrast, the $\delta^{15}N$ values of NC and CC irons record the end stage of thermal evolution of "first-generation" planetesimals, culminating with core-mantle differentiation. The distinct $\delta^{15}N$ values of NC and CC irons likely indicate differences in the N compositions of "first-generation" planetesimals in the inner and outer parts of the disk. Since differentiated "first-generation" planetesimals are the primary building blocks of terrestrial planets, the distinct N isotopic compositions of NC and CC irons can also be used to trace the origin of N on Earth.

4.8. Origin of N in Earth

Nucleosynthetic anomalies of several non-volatile elements suggest that Earth primarily grew from NC materials, with only a small contribution from the CC reservoir (~4%; Burkhardt et al., 2021)). The presence of N in NC IMPBs, the "first-generation" planetesimals in the inner solar system, suggests that N was present in the building blocks of terrestrial planets right from the onset of solar system formation (Grewal et al., 2021c). The contribution of these planetesimals to the N inventory of Earth can be gauged by comparing their N abundances and isotopic compositions with those of terrestrial reservoirs. Bulk silicate Earth contains ~2.8 μg of N per g of BSE, with ~1 μg/g residing in the atmosphere and ~1.8 μg/g still in the mantle (Fig. 1) (Hirschmann, 2018). The N inventory of the Earth's core is poorly constrained. Studies tracking the fate of N during terrestrial planet formation suggest a few tens of μg/g of N in the core (Speelmanns et al., 2019; Grewal et al., 2021b). This suggests that bulk Earth, akin to NC IMPBs, is extremely N-depleted. Therefore, it is likely that the N isotopic compositions of its constituent reservoirs, especially the non-core reservoirs, could preserve the signature of the N accreted from the "first generation" planetesimals in the inner solar system.

The $\delta^{15}N$ value of Earth's atmosphere is 0 ‰, whereas its value in the mantle is heterogenous. The $\delta^{15}N$ value of the convecting mantle, based on the analysis of mid-ocean ridge basalts, is −5 ‰, whereas the $\delta^{15}N$ value of Earth's primordial deep mantle, based on the N isotopic composition of peridotitic diamonds, could be much lower (<−40 ‰) (Fig. 1) (Cartigny and Marty, 2013). A ^{15}N-poor nature of Earth's primordial deep mantle suggests that the N isotopic composition of the interiors of the terrestrial planets is biased towards the accretion of ^{15}N-poor materials. However, the deep mantle is poorly sampled in Earth's rock record and its contribution to the overall N budget of the mantle remains poorly constrained. Importantly, the $\delta^{15}N$ value of the primordial mantle is significantly lower than that of enstatite chondrites (−21.1 ± 4.3 ‰). Mars grew rapidly within 1–2 Ma after CAIs (Dauphas and Pourmand, 2011), and the building blocks of Earth likely formed within similar timescales (Rubie et al., 2011; Weidenschilling, 2011). These rapid growth timescales are similar to the accretion ages of NC IMPBs. The mean $\delta^{15}N$ value of NC IMPBs, based on volatile un-depleted NC irons (IC, IIAB, IIIAB, and IIIE), is −82.3 ± 3.0 ‰. We note that the mean value could be higher, if the contributions of the N-depleted group IVA ($\delta^{15}N$ = − 28.9 ± 5.2 ‰) and of ungrouped NC irons (whose magamtic vs. non-magmatic origins are poorly understood) are considered. Either way, in comparison with the N isotopic composition of Earth's primordial mantle, NC IMPBs appear to be substantially ^{15}N-poor. This suggests dilution of the N isotopic composition of the primordial mantle by mixing with ^{15}N-rich materials during the later magma ocean events or through to the later infiltration of ^{15}N-rich materials via subduction over geological timescales. The early accreted ^{15}N-poor nitrogen may still be stored in the deep mantle, or it may have

segregated into Earth's core or lost to space during atmospheric loss caused by impacts. The ^{15}N-rich nature of Earth's present-day atmosphere and upper mantle relative to its deep interior suggests a significant contribution of CC materials (Fig. 1). It has been suggested that the N isotopic composition of Earth's atmosphere has evolved by the mixing of isotopically light N degassed from the Earth's mantle over geological timescales (Cartigny and Marty, 2013). Consequently, the δ^{15}N value of Earth's primordial atmosphere (>0‰) could have been even more biased towards the accretion of ^{15}N-rich materials. Since Earth had a protracted growth history, it cannot be distinguished solely from N whether these CC materials had IMPB or chondrite parent body origin. However, establishing the inventory of less-depleted volatiles, such as carbon and water, in the bulk silicate Earth suggests that the delivery of ^{15}N-rich nitrogen could have occurred through the accretion of chondrite-like materials (Marty, 2012; Alexander et al., 2012; Grewal et al., 2024a). Earth's core primarily grew through the direct accretion of the cores of planetesimals and planetary embryos, which formed in the inner solar system (Karato and Rama Murthy, 1997; Rubie et al., 2011). Since these bodies likely grew on timescales similar to those of NC IMPBs, the N isotopic composition of Earth's core could be significantly ^{15}N-poor relative to its atmosphere and convecting mantle.

5. Conclusions

The N isotopic compositions of iron meteorites have emerged as a promising proxy for constraining the origin of volatiles on Earth. However, our limited understanding of N isotope fractionation during core crystallization has restricted its utility. In this study, we performed high pressure, high-temperature experiments to determine the equilibrium fractionation of N isotopes between S-free solid and S-bearing liquid metal under conditions relevant to core crystallization within planetesimals. Our experimental data reveal that S-bearing liquid metals are modestly ^{15}N-poor relative to the S-free solid metals, and the extent of N isotope fractionation increases with the S content of the liquid metal. Consequently, the unsampled (S-rich) fractions of the parent cores were slightly ^{15}N-poor compared to the sampled fractions. However, the small magnitude of N isotope fractionation between solid and liquid metal ($\Delta^{15}N^{solid–liquid} = \delta^{15}N^{solid} - \delta^{15}N^{liquid} = 0.3$ ‰ and 1.2 ‰) suggests that the N isotopic compositions of iron meteorites were not significantly altered by solid metal-liquid metal equilibration during core crystallization. Importantly, these alterations are much lower than the inter-group variations of δ^{15}N values among magmatic iron groups. This, combined with the siderophile character of N and limited equilibrium N isotope fractionation during core-mantle differentiation, suggests that iron meteorites accurately reflect the bulk N isotopic compositions of their parent bodies and serve as a reliable proxy for tracing the origin of N on Earth.

Grouped NC iron meteorites are systematically ^{15}N-poor relative to their CC counterparts. In addition, their δ^{15}N values are lower by 50–70 ‰ lower than those of NC chondrites. Unlike the variation in the N isotopic compositions of NC and CC chondrites, which can be attributed to comparable geophysical processes affecting common organic precursors, the ^{15}N-poor nature of NC irons relative to CC irons likely represents the distinct N isotopic compositions of the earliest inner and outer solar system planetesimals. The N isotopic composition of Earth's primordial mantle ($\delta^{15}N = <-40$ ‰) suggests that it retains the imprint of early accretion of ^{15}N-poor NC iron meteorite parent body-like planetesimals. This early accreted ^{15}N-poor nitrogen is either stored in the deep mantle, segregated into Earth's core, or was lost to space. This signature was subsequently overprinted by the later accretion and admixing of CC materials, which is reflected in the relatively ^{15}N-rich nature of Earth's atmosphere ($\delta^{15}N = 0$) and convecting mantle ($\delta^{15}N = -5$ ‰).

CRediT authorship contribution statement

Damanveer S. Grewal: Writing – original draft, Visualization, Validation, Resources, Project administration, Methodology, Investigation, Funding acquisition, Formal analysis, Data curation, Conceptualization. **Surjyendu Bhattacharjee:** Writing – review & editing, Visualization, Validation, Investigation, Formal analysis, Data curation. **Gabriel-Darius Mardaru:** Investigation. **Paul D. Asimow:** Writing – review & editing, Validation, Resources.

Data availability

Data are available through zenodo at https://doi.org/10.5281/zenodo.13988625.

Declaration of competing interest

The authors declare that they have no known competing financial interests or personal relationships that could have appeared to influence the work reported in this paper.

Acknowledgements

We thank Peng Ni, Mathieu Roskosz, and Associate Editor Béatrice Luais for their constructive reviews. Amrita P. Vyas is thanked for improving the clarity of our communication. This study was funded by a Barr Foundation postdoctoral fellowship by Caltech and startup funds from ASU to D.S.G. Chi Ma is thanked for his help during the EPMA analyses and Michael Mathuri is thanked for assistance with EA-IRMS analyses. Alex Sessions, Ed Stolper, and George Rossman are acknowledged for granting access to their laboratories.

Appendix A. Supplementary material

The supplementary file includes four tables: Supplementary Table 1 lists the compositions of the starting materials, Supplementary Tables 2 and 3 provide the compositions of the solid and liquid metals, respectively, and Supplementary Table 4 presents the nitrogen isotope compositions of the reference materials. Supplementary material to this article can be found online at https://doi.org/10.1016/j.gca.2024.11.011.

References

Alexander, C.M.O., Bowden, R., Fogel, M.L., Howard, K.T., Herd, C.D.K., Nittler, L.R., 2012. The Provenances of Asteroids, and Their Contributions to the Volatile Inventories of the Terrestrial Planets. Science 337, 721–723.

Alexander, C.M.O., Cody, G.D., De Gregorio, B.T., Nittler, L.R., Stroud, R.M., 2017. The nature, origin and modification of insoluble organic matter in chondrites, the major source of Earth's C and N. Geochemistry 77, 227–256.

Alexander, C.M.O.D., Fogel, M., Yabuta, H., Cody, G.D., 2007. The origin and evolution of chondrites recorded in the elemental and isotopic compositions of their macromolecular organic matter. Geochim. Cosmochim. Acta 71, 4380–4403.

Alexander, C.M.O., Greenwood, R.C., Bowden, R., Gibson, J.M., Howard, K.T., Franchi, I. A., 2018. A mutli-technique search for the most primitive CO chondrites. Geochim. Cosmochim. Acta 221, 406–420.

Alexander, C.M.O.D., Howard, K.T., Bowden, R., Fogel, M.L., 2013. The classification of CM and CR chondrites using bulk H, C and N abundances and isotopic compositions. Geochim. Cosmochim. Acta 123, 244–260.

Alexander, C.M.O., Russell, S.S., Arden, J.W., Ash, R.D., Grady, M.M., Pillinger, C.T., 1998. The origin of chondritic macromolecular organic matter: a carbon and nitrogen isotope study. Meteorit. Planet. Sci. 33, 603–622.

Bourdon, B., Roskosz, M., Hin, R.C., 2018. Isotope tracers of core formation. Earth Sci. Rev. 181, 61–81.

Brearley, A.J., 2006. The action of water. In: Lauretta, D.S., McSween Jr., H.Y. (Eds.), Meteorites and the Early Solar System II. The University of Arizona Press, Tucson, pp. 587–624.

Broadley, M.W., Bekaert, D.V., Piani, L., Füri, E., Marty, B., 2022. Origin of life-forming volatile elements in the inner Solar System. Nature 611, 245–255.

Buchwald, V.F., 1975. Handbook of Iron Meteorites: Their History, Distribution, Composition and Structure. University of California Press.

Burkhardt, C., Spitzer, F., Morbidelli, A., Budde, G., Render, J.H., Kruijer, T.S., Kleine, T., 2021. Terrestrial planet formation from lost inner solar system material. Sci. Adv. 7, 7601.
Campbell, A.J., Humayun, M., 2005. Compositions of group IVB iron meteorites and their parent melt. Geochim. Cosmochim. Acta 69, 4733–4744.
Cartigny, P., Marty, B., 2013. Nitrogen Isotopes and Mantle Geodynamics: The Emergence of Life and the Atmosphere-Crust-Mantle Connection. Elements 9, 359–366.
Chabot, N.L., 2004. Sulfur contents of the parental metallic cores of magmatic iron meteorites. Geochim. Cosmochim. Acta 68, 3607–3618.
Chabot, N.L., Campbell, A.J., Jones, J.H., Humayun, M., Vern, L.H., 2006. The influence of carbon on trace element partitioning behavior. Geochim. Cosmochim. Acta 70, 1322–1335.
Chabot, N.L., Jones, J.H., 2003. The parameterization of solid metal-liquid metal partitioning of siderophile elements. Meteorit. Planet. Sci. 38, 1425–1436.
Chabot, N.L., Wollack, E.A., McDonough, W.F., Ash, R.D., Saslow, S.A., 2017. Experimental determination of partitioning in the Fe-Ni system for applications to modeling meteoritic metals. Meteorit. Planet. Sci. 52, 1133–1145.
Chabot, N.L., Zhang, B., 2022. A revised trapped melt model for iron meteorites applied to the IIIAB group. Meteorit. Planet. Sci. 57, 200–227.
Cody, G.D., Alexander, C.M.O., Yabuta, H., Kilcoyne, A.L.D., Araki, T., Ade, H., Dera, P., Fogel, M., Militzer, B., Mysen, B.O., 2008. Organic thermometry for chondritic parent bodies. Earth Planet. Sci. Lett. 272, 446–455.
Dalou, C., Hirschmann, M.M., von der Handt, A., Mosenfelder, J., Armstrong, L.S., 2017. Nitrogen and carbon fractionation during core–mantle differentiation at shallow depth. Earth Planet. Sci. Lett. 458, 141–151.
Dalou, C., Füri, E., Deligny, C., Piani, L., Caumon, M.-C., Laumonier, M., Boulliung, J., Edén, M., 2019. Redox control on nitrogen isotope fractionation during planetary core formation. Proc. Natl. Acad. Sci. 116, 14485–14494.
Dasgupta, R., Grewal, D.S., 2019. Origin and Early Differentiation of Carbon and Associated Life-Essential Volatile Elements on Earth. In: Orcutt, B., Daniel, I., Dasgupta, R. (Eds.), Deep Carbon: past to Present. Cambridge University Press, pp. 4–39.
Dauphas, N., 2017. The isotopic nature of the Earth's accreting material through time. Nature 541, 521–524.
Dauphas, N., Pourmand, A., 2011. Hf–W–Th evidence for rapid growth of Mars and its status as a planetary embryo. Nature 473, 489–492.
Elkins-Tanton, L.T., Weiss, B.P., Zuber, M.T., 2011. Chondrites as samples of differentiated planetesimals. Earth Planet. Sci. Lett. 305, 1–10.
Foustoukos, D.I., Alexander, D., Cody, G.D., 2021. H and N systematics in thermally altered chondritic insoluble organic matter: an experimental study. Geochim. Cosmochim. Acta 300, 44–64.
Franchi, I.A., Wright, I.P., Pillinger, C.T., 1993. Constraints on the formation conditions of iron meteorites based on concentrations and isotopic compositions of nitrogen. Geochim. Cosmochim. Acta 57, 3105–3121.
Füri, E., Marty, B., 2015. Nitrogen isotope variations in the Solar System. Nat. Geosci. 8, 515–522.
Gaskell, D.R., Laughlin, D.E., 2017. Introduction to the Thermodynamics of Materials, sixth ed. CRC Press.
Goldstein, J.I., Scott, E.R.D., Chabot, N.L., 2009. Iron meteorites: Crystallization, thermal history, parent bodies, and origin. Chem. Erde 69, 293–325.
Grady, M.M., Wright, I.P., Carr, L.P., Pillinger, C.T., 1986. Compositional differences in enstatite chondrites based on carbon and nitrogen stable isotope measurements. Geochim. Cosmochim. Acta 50, 2799–2813.
Grewal, D.S., 2022. Origin of Nitrogen Isotopic Variations in the Rocky Bodies of the Solar System. Astrophys. J. 937, 123.
Grewal, D.S., Asimow, P.D., 2023. Origin of the superchondritic carbon/nitrogen ratio of the bulk silicate Earth – an outlook from iron meteorites. Geochim. Cosmochim. Acta 344, 146–159.
Grewal, D.S., Dasgupta, R., Holmes, A.K., Costin, G., Li, Y., Tsuno, K., 2019a. The fate of nitrogen during core-mantle separation on Earth. Geochim. Cosmochim. Acta 251, 87–115.
Grewal, D.S., Dasgupta, R., Sun, C., Tsuno, K., Costin, G., 2019b. Delivery of carbon, nitrogen, and sulfur to the silicate Earth by a giant impact. Sci. Adv. 5, eaau3669.
Grewal, D.S., Dasgupta, R., Farnell, A., 2020. The speciation of carbon, nitrogen, and water in magma oceans and its effect on volatile partitioning between major reservoirs of the Solar System rocky bodies. Geochim. Cosmochim. Acta 280, 281–301.
Grewal, D.S., Dasgupta, R., Aithala, S., 2021a. The effect of carbon concentration on its core-mantle partitioning behavior in inner Solar System rocky bodies. Earth Planet. Sci. Lett. 571, 117090.
Grewal, D.S., Dasgupta, R., Hough, T., Farnell, A., 2021b. Rates of protoplanetary accretion and differentiation set nitrogen budget of rocky planets. Nat. Geosci. 14, 369–376.
Grewal, D.S., Dasgupta, R., Marty, B., 2021c. A very early origin of isotopically distinct nitrogen in inner Solar System protoplanets. Nat. Astron 5, 356–364.
Grewal, D.S., Seales, J.D., Dasgupta, R., 2022a. Internal or external magma oceans in the earliest protoplanets – perspectives from nitrogen and carbon fractionation. Earth Planet. Sci. Lett. 598, 117847.
Grewal, D.S., Sun, T., Aithala, S., Hough, T., Dasgupta, R., Yeung, L.Y., Schauble, E.A., 2022b. Limited nitrogen isotopic fractionation during core-mantle differentiation in rocky protoplanets and planets. Geochim. Cosmochim. Acta 338, 347–364.
Grewal, D.S., Miyazaki, Y., Nie, N.X., 2024a. Contribution of the Moon-forming Impactor to the Volatile Inventory in the Bulk Silicate Earth. Planet Sci J 5, 181.
Grewal, D.S., Nie, N.X., Zhang, B., Izidoro, A., Asimow, P.D., 2024b. Accretion of the earliest inner Solar System planetesimals beyond the water snowline. Nat. Astron 8, 290–297.
Halliday, A.N., 2013. The origins of volatiles in the terrestrial planets. Geochim. Cosmochim. Acta 105, 146–171.
Hashizume, K., Sugiura, N., 1995. Nitrogen isotopes in bulk ordinary chondrites. Geochim. Cosmochim. Acta 59, 4057–4069.
Hevey, P.J., Sanders, I.S., 2006. A model for planetesimal meltdown by 26 Al and its implications for meteorite parent bodies. Meteorit. Planet. Sci. 41, 95–106.
Hilton, C.D., Ash, R.D., Walker, R.J., 2022. Chemical characteristics of iron meteorite parent bodies. Geochim. Cosmochim. Acta 318, 112–125.
Hinomura, T., Nasu, S., 1998. A study of Fe-N alloy systems. Hyperfine Interact. 111, 221–226.
Hirschmann, M.M., 2016. Constraints on the early delivery and fractionation of Earth's major volatiles from C/H, C/N, and C/S ratios. Am. Mineral. 101, 540–553.
Hirschmann, M.M., 2018. Comparative deep Earth volatile cycles: the case for C recycling from exosphere/mantle fractionation of major (H2O, C, N) volatiles and from H2O/Ce, CO2/Ba, and CO2/Nb exosphere ratios. Earth Planet. Sci. Lett. 502, 262–273.
Hirschmann, M.M., Bergin, E.A., Blake, G.A., Ciesla, F.J., Li, J., 2021. Early volatile depletion on planetesimals inferred from C–S systematics of iron meteorite parent bodies. Proc. Natl. Acad. Sci. 118.
Huss, G.R., Rubin, A.E., Grossman, J.N., 2006. Thermal Metamorphism in Chondrites. In: Meteorites and the early solar system II (eds. D. S. Lauretta and H. Y. McSween Jr.). University of Arizona Press. pp. 567–586.
Jackson, C.R.M., Cottrell, E., Du, Z., Bennett, N.R., Fei, Y., 2021. High pressure redistribution of nitrogen and sulfur during planetary stratification. Geochem. Perspect. Lett. 37–42.
Javoy, M., Pineau, F., Delorme, H., 1986. Carbon and nitrogen isotopes in the mantle. Chem. Geol. 57, 41–62.
Javoy, M., Kaminski, E., Guyot, F., Andrault, D., Sanloup, C., Moreira, M., Labrosse, S., Jambon, A., Agrinier, P., Davaille, A., Jaupart, C., 2010. The chemical composition of the Earth: Enstatite chondrite models. Earth Planet. Sci. Lett. 293, 259–268.
Kaminski, E., Limare, A., Kenda, B., Chaussidon, M., 2020. Early accretion of planetesimals unraveled by the thermal evolution of the parent bodies of magmatic iron meteorites. Earth Planet. Sci. Lett. 548, 116469.
Karato, S.-I., Rama, M.V., 1997. Core formation and chemical equilibrium in the Earth Physical considerations. Phys. Earth Planet. In. 100, 61–79.
Keil, K., Haack, H., Scott, E.R.D., 1994. Catastrophic fragmentation of asteroids: evidence from meteorites. Planet. Space Sci. 42, 1109–1122.
Kojima, Y., Inouye, M., Yamada, Y., 1975. Solubility and diffusivity of nitrogen in liquid iron-nickel and iron-cobalt alloys at 1600℃. Trans. Iron Steel Institute of Japan 15, 599–605.
Kruijer, T.S., Touboul, M., Fischer-Godde, M., Bermingham, K.R., Walker, R.J., Kleine, T., 2014. Protracted core formation and rapid accretion of protoplanets. Science 344, 1150–1154.
Kruijer, T.S., Burkhardt, C., Budde, G., Kleine, T., 2017. Age of Jupiter inferred from the distinct genetics and formation times of meteorites. Proc. Natl. Acad. Sci. 114, 6712–6716.
Kunze, H.-D., Schürmann, E., Parlee, N.A.D., 1970. Influence of temperature and equivalent effect of added elements on the solubility, activity, and activity coefficient of nitrogen in liquid iron. Metallurgical Transactions 1, 281–290.
Lauretta, D.S., Connolly, H.C., Aebersold, J.E., Alexander, C.M.O., Ballouz, R., Barnes, J. J., Bates, H.C., Bennett, C.A., Blanche, L., Blumenfeld, E.H., Clemett, S.J., Cody, G. D., DellaGiustina, D.N., Dworkin, J.P., Eckley, S.A., Foustoukos, D.I., Franchi, I.A., Glavin, D.P., Greenwood, R.C., Haenecour, P., Hamilton,V.E., Hill, D.H., Hiroi, T., Ishimaru, K., Jourdan, F., Kaplan, H.H., Keller, L.P., King, A.J., Koefoed, P., Kontogiannis, M.K., Le, L., Macke, R.J., McCoy, T.J., Milliken, R.E., Najorka, J., Nguyen, A N., Pajola, M., Polit, A.T., Righter, K., Roper, H.L., Russell, S.S., Ryan, A. J., Sandford, S.A., Schofield, P.F., Schultz, C.D., Seifert, L.B., Tachibana, S., Thomas-Keprta, K.L., Thompson, M.S., Tu, V., Tusberti, F., Wang, K., Zega, T.J., Wolner, C.W. V., 2024. Asteroid (101955) Bennu in the laboratory: Properties of the sample collected by OSIRIS-REx. Meteorit Planet Sci.
Li, Y., Marty, B., Shcheka, S., Zimmermann, L., Keppler, H., 2016. Nitrogen isotope fractionation during terrestrial core-mantle separation. Geochem. Perspect. Lett. 138–147.
Li, Y., Wiedenbeck, M., Monteleone, B., Dasgupta, R., Costin, G., Gao, Z., Lu, W., 2023. Nitrogen and carbon fractionation in planetary magma oceans and origin of the superchondritic C/N ratio in the bulk silicate Earth. Earth Planet. Sci. Lett. 605, 118032.
Lichtenberg, T., Drążkowska, J., Schönbächler, M., Golabek, G.J., Hands, T.O., 2021. Bifurcation of planetary building blocks during Solar System formation. Science 1979 (371), 365–370.
Luais, B., 2007. Isotopic fractionation of germanium in iron meteorites: Significance for nebular condensation, core formation and impact processes. Earth Planet. Sci. Lett. 262, 21–36.
Marty, B., 2012. The origins and concentrations of water, carbon, nitrogen and noble gases on Earth. Earth Planet. Sci. Lett. 313–314, 56–66.
Mathew, K.J., Palma, R.L., Marti, K., Lavielle, B., 2000. Isotopic signatures and origin of nitrogen in IIE and IVA iron meteorites. Geochim. Cosmochim. Acta 64, 545–557.
Matthes, M., Fischer-Gödde, M., Kruijer, T.S., Kleine, T., 2018. Pd-Ag chronometry of IVA iron meteorites and the crystallization and cooling of a protoplanetary core. Geochim. Cosmochim. Acta 220, 82–95.
Mehrer, H., 2007. Diffusion in Solids. Springer, Berlin Heidelberg, Berlin, Heidelberg.

Monnereau, M., Toplis, M.J., Baratoux, D., Guignard, J., 2013. Thermal history of the H-chondrite parent body: Implications for metamorphic grade and accretionary time-scales. Geochim. Cosmochim. Acta 119, 302–321.
Murty, S.V.S., Marti, K., 1994. Nitrogen isotopic signatures in Cape York: Implications for formation of Group III A irons. Geochim. Cosmochim. Acta 58, 1841–1848.
Ni, P., Chabot, N.L., Ryan, C.J., Shahar, A., 2020. Heavy iron isotope composition of iron meteorites explained by core crystallization. Nat. Geosci. 13, 611–615.
Ni, P., Zhan, Y., Chabot, N.L., Ryan, C.J., Zhu, K., Nie, N.X., Shirey, S.B., Shahar, A., 2024. Copper isotope fractionation during asteroid core solidification. Geochem. Perspect. Lett. 31, 49–53.
Oikawa, H., 1982. Review on Lattice Diffusion of Substitutional Impurities in Iron-A Summary Report. Tech. Reports, Tohuku University 47, 215.
Pathak, D., Dasgupta, R., 2024. Nitrogen inventory of iron meteorite parent bodies constrained by nitrogen partitioning between Fe-rich solid and liquid alloys. Geochim. Cosmochim. Acta 371, 199–213.
Pearson, V.K., Sephton, M.A., Franchi, I.A., Gibson, J.M., Gilmour, I., 2006. Carbon and nitrogen in carbonaceous chondrites: Elemental abundances and stable isotopic compisitions. Meteorit. Planet. Sci. 41, 1899–1918.
Pepin, R.O., Becker, R.H., 1982. Nitrogen Isotopes in Iron Meteorites. Meteoritics 17, 269.
Ponganis, K.V., Marti, K., 2007. Nitrogen components in IAB/IIICD iron meteorites. Meteorit. Planet. Sci. 42, 331–346.
Prombo, C.A., Clayton, R.N., 1993. Nitrogen isotopic compositions of iron meteorites. Geochim. Cosmochim. Acta 57, 3749–3761.
Rubie, D.C., Frost, D.J., Mann, U., Asahara, Y., Nimmo, F., Tsuno, K., Kegler, P., Holzheid, A., Palme, H., 2011. Heterogeneous accretion, composition and core-mantle differentiation of the Earth. Earth Planet. Sci. Lett. 301, 31–42.
Sahijpal, S., Soni, P., Gupta, G., 2007. Numerical simulations of the differentiation of accreting planetesimals with 26Al and 60Fe as the heat sources. Meteorit. Planet. Sci. 42, 1529–1548.
Sephton, M.A., Verchovsky, A.B., Bland, P.A., Gilmour, I., Grady, M.M., Wright, I.P., 2003. Investigating the variations in carbon and nitrogen isotopes in carbonaceous chondrites. Geochim. Cosmochim. Acta 67, 2093–2108.
Shi, L., Lu, W., Kagoshima, T., Sano, Y., Gao, Z., Du, Z., Liu, Y., Fei, Y., Li, Y., 2022. Nitrogen isotope evidence for Earth's heterogeneous accretion of volatiles. Nat. Commun. 13, 4769.
Speelmanns, I.M., Schmidt, M.W., Liebske, C., 2018. Nitrogen Solubility in Core Materials. Geophys. Res. Lett. 45, 7434–7443.
Speelmanns, I.M., Schmidt, M.W., Liebske, C., 2019. The almost lithophile character of nitrogen during core formation. Earth Planet. Sci. Lett. 510, 186–197.
Sturtz, C., Limare, A., Tait, S., Kaminski, É., 2022b. Birth and Decline of Magma Oceans in Planetesimals: 2. Structure and Thermal History of Early Accreted Small Planetary Bodies. J. Geophys. Res. Planets 127.
Sturtz, C., Limare, A., Chaussidon, M., Kaminski, É., 2022a. Structure of differentiated planetesimals: A chondritic fridge on top of a magma ocean. Icarus 385, 115100.
Suer, T.-A., Jackson, C., Grewal, D.S., Dalou, C., Lichtenberg, T., 2023. The distribution of volatile elements during rocky planet formation. Front. Earth Sci. (Lausanne) **11**.
Sugiura, N., 1998. Ion probe measurements of carbon and nitrogen in iron meteorites. Meteorit. Planet. Sci. 33, 393–409.
Sugiura, N., Brar, N.S., Strangway, D.W., Matsui, T., 1984. Degassing of meteorite parent bodies. J. Geophys. Res. 89, B641.
Sugiura, N., Fujiya, W., 2014. Correlated accretion ages and ε 54 Cr of meteorite parent bodies and the evolution of the solar nebula. Meteorit. Planet. Sci. 49, 772–787.
Sugiura, N., Arkani-Hamed, J., Strangway, D.W., 1986. Possible transport of carbon in meteorite parent bodies. Earth Planet. Sci. Lett. 78, 148–156.
Tsuno, K., Grewal, D.S., Xu, V., Leinbach, L., Leinenweber, K., Wittmann, A., Shim, S., 2024. The Effect of Nitrogen on the Dihedral Angle Between Fe−Ni Melt and Ringwoodite: Implications for the Nitrogen Deficit in the Bulk Silicate Earth. Geophys Res Lett 51.
Tsuno, K., Grewal, D.S., Dasgupta, R., 2018. Core-mantle fractionation of carbon in Earth and Mars: The effects of sulfur. Geochim. Cosmochim. Acta 238, 477–495.
Wasson, J.T., 1999. Trapped melt in IIIAB irons; solid/liquid elemental partitioning during the fractionation of the IIIAB magma. Geochim. Cosmochim. Acta 63, 2875–2889.
Wasson, J.T., Huber, H., 2006. Compositional trends among IID irons; their possible formation from the P-rich lower magma in a two-layer core. Geochim. Cosmochim. Acta 70, 6153–6167.
Wasson, J.T., Richardson, J.W., 2001. Fractionation trends among IVA iron meteorites: contrasts with IIIAB trends. Geochim. Cosmochim. Acta 65, 951–970.
Weidenschilling, S.J., 2011. Initial sizes of planetesimals and accretion of the asteroids. Icarus 214, 671–684.
Yabuta H., Cody G. D., Engrand C., Kebukawa Y., De Gregorio B., Bonal L., Remusat L., Stroud R., Quirico E., Nittler L., Hashiguchi M., Komatsu M., Okumura T., Mathurin J., Dartois E., Duprat J., Takahashi Y., Takeichi Y., Kilcoyne D., Yamashita S., Dazzi A., Deniset-Besseau A., Sandford S., Martins Z., Tamenori Y., Ohigashi T., Suga H., Wakabayashi D., Verdier-Paoletti M., Mostefaoui S., Montagnac G., Barosch J., Kamide K., Shigenaka M., Bejach L., Matsumoto M., Enokido Y., Noguchi T., Yurimoto H., Nakamura T., Okazaki R., Naraoka H., Sakamoto K., Connolly H. C., Lauretta D. S., Abe M., Okada T., Yada T., Nishimura M., Yogata K., Nakato A., Yoshitake M., Iwamae A., Furuya S., Hatakeda K., Miyazaki A., Soejima H., Hitomi Y., Kumagai K., Usui T., Hayashi T., Yamamoto D., Fukai R., Sugita S., Kitazato K., Hirata Naru, Honda R., Morota T., Tatsumi E., Sakatani N., Namiki N., Matsumoto K., Noguchi R., Wada K., Senshu H., Ogawa K., Yokota Y., Ishihara Y., Shimaki Y., Yamada M., Honda C., Michikami T., Matsuoka M., Hirata Naoyuki, Arakawa M., Okamoto C., Ishiguro M., Jaumann R., Bibring J.-P., Grott M., Schröder S., Otto K., Pilorget C., Schmitz N., Biele J., Ho T.-M., Moussi-Soffys A., Miura A., Noda H., Yamada T., Yoshihara K., Kawahara K., Ikeda H., Yamamoto Y., Shirai K., Kikuchi S., Ogawa N., Takeuchi H., Ono G., Mimasu Y., Yoshikawa K., Takei Y., Fujii A., Iijima Y., Nakazawa S., Hosoda S., Iwata T., Hayakawa M., Sawada H., Yano H., Tsukizaki R., Ozaki M., Terui F., Tanaka S., Fujimoto M., Yoshikawa M., Saiki T., Tachibana S., Watanabe S., Tsuda Y., 2023. Macromolecular organic matter in samples of the asteroid (162173) Ryugu. Science (1979) 379, 25.
Yang, J., Goldstein, J.I., Scott, E.R.D., 2007. Iron meteorite evidence for early formation and catastrophic disruption of protoplanets. Nature 446, 888–891.
Yang, J., Goldstein, J.I., Scott, E.R.D., 2008. Metallographic cooling rates and origin of IVA iron meteorites. Geochim. Cosmochim. Acta 72, 3043–3061.
Young, E.D., Manning, C.E., Schauble, E.A., Shahar, A., Macris, C.A., Lazar, C., Jordan, M., 2015. High-temperature equilibrium isotope fractionation of non-traditional stable isotopes: experiments, theory, and applications. Chem. Geol. 395, 176–195.
Zhang, B., Chabot, N.L., Rubin, A.E., 2022. Compositions of carbonaceous-type asteroidal cores in the early solar system. Sci. Adv. 8, 5781.
Zhang, B., Chabot, N.L., Chabot, N.L., 2024. Compositions of iron-meteorite parent bodies: constraints on the structure of the protoplanetary disk. Proc. Natl. Acad. Sci. 121.